Tuning the photoluminescence properties of SLE- and MRL-active tricarbonylrhenium(I) complexes through minor structural changes of the organic ligand

Alexandre Poirot, Nadine Leygue, Béatrice Delavaux-Nicot, Nathalie Saffon-Merceron, Clémence Allain, Eric Benoist, Suzanne Fery-Forgues

Tuning the photoluminescence properties of SLE- and MRL-active tricarbonylrhenium(I) complexes through minor structural changes of the organic ligand

Alexandre Poirot,[a] Nadine Leygue,[a] Béatrice Delavaux-Nicot,[b] Nathalie Saffon-Merceron,[c] Clémence Allain,[d] Eric Benoist [a] and Suzanne Fery-Forgues *[a]

[a] *SPCMIB, CNRS UMR 5068, Université de Toulouse III Paul Sabatier, 118 route de Narbonne, 31062 Toulouse cedex 9, France*
[b] *Laboratoire de Chimie de Coordination, CNRS (UPR 8241), Université de Toulouse (UPS, INPT), 205 route de Narbonne, 31077 Toulouse Cedex 4, France*
[c] *Service Diffraction des Rayons X, Institut de Chimie de Toulouse, ICT- UAR 2599, Université de Toulouse III Paul Sabatier, 118 route de Narbonne, 31062 Toulouse cedex 9, France*
[d] *Université Paris-Saclay, ENS Paris-Saclay, CNRS, Photophysique et Photochimie Supramoléculaires et Macromoléculaires 91190 Gif-sur-Yvette, France*

* Corresponding author.
E-mail address: suzanne.fery-forgues@univ-tlse3.fr

Keywords:
Transition metal complex
Rhenium
Solid-state luminescence enhancement
Aggregation-Induced Emission
Mechanoresponsive luminescence

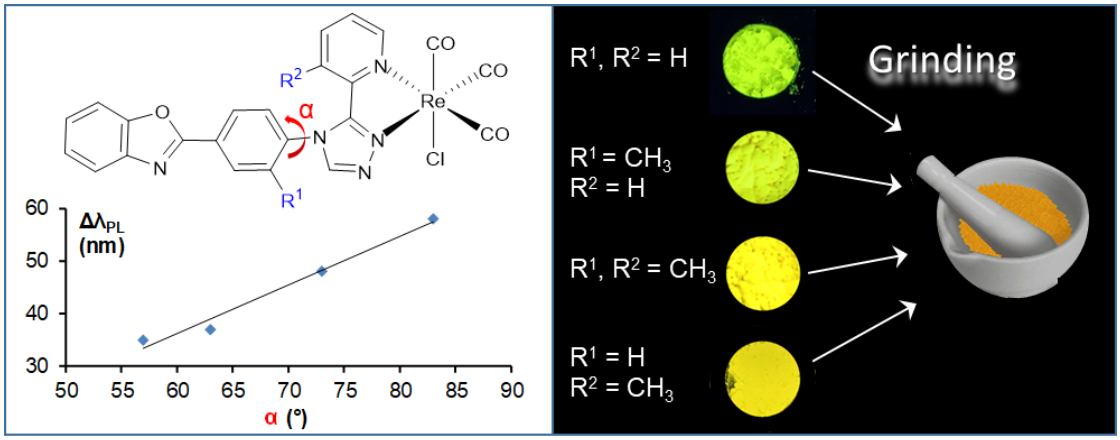

Highlights

The complexes differ by the presence of methyl groups on their organic ligand
The substitution pattern influences the molecular geometry and crystal packing mode
Therefore, it impacts the solid-state luminescence and mechanochromic properties
Remarkably, the phenyl-pyta angle correlates well with the MRL effect amplitude

Abstract

Solid-state luminescence properties depend on numerous parameters, including the molecular geometry and the intermolecular interactions that take place in the solid. To clarify the role played by these parameters on the photoluminescence (PL) properties of tricarbonylrhenium(I) complexes, four molecules incorporating a 3-(2-pyridyl)-1,2,4-triazole (pyta) ligand with appended phenylbenzoxazole (PBO) unit were compared. One or two methyl groups were inserted at different places of the organic ligand of the parent compound **RePBO**, resulting in three new complexes **RePBO-Me1**, **RePBO-Me2** and **RePBO-Me3**. As shown by NMR, the presence of the methyl group(s) induced some changes in

molecular flexibility, but the electronic effects were relatively weak. As a result, the electrochemical and optical properties were little impacted, and the four complexes behaved almost similarly in organic solution, in agreement with theoretical calculations. In contrast, marked differences appeared between the complexes when considering the aggregation-induced emission (AIE) effect, mainly due to the formation of tiny microcrystals in aqueous medium. In the same way, the three methylated complexes in the form of microcrystalline powders showed clear crystallization-induced emission enhancement (CIEE) with respect to solutions, but with distinct characteristics. They emitted less intensely and at longer wavelengths than the unsubstituted complex. Most likely, the methyl groups strongly affect the geometry and the packing mode of the molecules in the crystals, which influence the PL properties in the solid state. After grinding the powders, the emission spectra of the three methylated complexes were shifted to the red, although this shift was weaker than that previously observed for **RePBO**. This effect was almost reversible after THF fuming. It was attributed to transitions between the crystalline and amorphous phases. Remarkably, in the amorphous phase where molecules regain their mobility, the emission differences between the four complexes almost disappeared. It was then concluded that the amplitude of the mechanoresponsive luminescence (MRL) effect strongly depends on the geometry of the molecules in the pristine powder. This study is one more step toward the rational design of photoluminescent tricarbonylrhenium(I) complexes. More generally, it is also a good example of how very small structural modifications can drastically govern the PL and MRL properties.

1. Introduction

Luminophores that exhibit good aggregation-induced emission (AIE) properties [1, 2] and, more widely speaking, solid-state luminescence enhancement (SLE) properties [3], *i.e.* whose emission is markedly enhanced in the aggregate and various solid states with respect to solutions, generate increasing attention given their numerous applications in the fields of bioimaging and luminescent materials. Closely related molecules with mechanoresponsive luminescence (MRL) properties, *i.e.* whose emission is sensitive to mechanical stimuli, are highly sought after for the fabrication of smart sensors, optoelectronic systems, and security devices [4–8]. Over the last twenty years, a considerable amount of experimental and theoretical work has established basic design criteria for these two types of molecules as far as organic compounds are considered. However, transition metal complexes are under-represented in these fields [6–13], although they have distinct advantages in terms of photostability and tuneability of the spectroscopic properties. Systematic studies to access their rational design are of great interest, but they are still rare. One reason is that both the molecular electronic system and the various intermolecular interactions that take place in the solid state control the SLE and MRL properties, and their respective contributions are difficult to unravel. This is especially true when it comes to the triplet state, which is the main contributor to the emission process in transition metal complexes.

Recently, our group has studied new photoluminescent tricarbonylrhenium(I) complexes, with particular attention to their SLE and MRL properties. These complexes incorporate a chloride ligand that endows them with good photochemical stability, and they are characterized by the presence of a pyridyl-triazole (pyta) moiety, an excellent chelator that exists in different isomer forms. Much easier to substitute than conventional pyridine-based derivatives, this bidentate ligand lends itself well to many chemical modifications. Neither SLE nor MRL effects were observed for a complex built from a 4-(2-pyridyl)-1,2,3-triazole moiety provided with an aromatic unit, whose organic ligand is almost planar [14]. In contrast, successive studies have shown the superiority of all complexes integrating the isomeric 3-(2-pyridyl)-1,2,4-triazole moiety, in relation to which the appended aromatic unit forms a large dihedral angle [15–18]. Among all the complexes studied, **RePBO** (Scheme 1) that incorporates a 2-phenylbenzoxazole (PBO) heterocycle, combines SLE and MRL effects in a spectacular way [15, 18]. In this molecule, the pyta moiety and the freely-rotating PBO unit are almost perpendicular to each other. It was proposed that this particular molecular geometry plays an important role in the solid-state luminescence properties.

In order to support this hypothesis with new evidence, and to better identify the key elements that govern the SLE and MRL properties of these tricarbonylrhenium(I) complexes, we imagined changing the geometry of **RePBO** through a very small modification of the molecular structure. No bulky substituents were to be introduced to avoid completely altering the crystal packing mode and

blocking the rotation. Besides, for the sake of comparison, the electron system of the molecules had to vary as little as possible. With this in mind, three new complexes inspired by **RePBO** were prepared by adding a methyl group on the phenyl ring of the PBO unit (**RePBO-Me1**), on the pyridyl ring (**RePBO-Me2**) and on both positions (**RePBO-Me3**) (Scheme 1). ^{1}H NMR spectroscopy provided information about the rotation of molecules in solution. The theoretical, electrochemical and spectroscopic studies confirmed that the electronic properties of the three new complexes in solution varied relatively little. This was no longer the case in the crystalline phase, where each compound has its own molecular geometry and packing mode. The solid-state luminescence properties were therefore different, and also well distinct from those of the parent compound. This study shows how minor modifications brought to the molecular structure of **RePBO** strongly influence the photophysics of the new complexes in the solid state. It contributes to a comprehensive understanding of the SLE and MRL properties for this family of complexes.

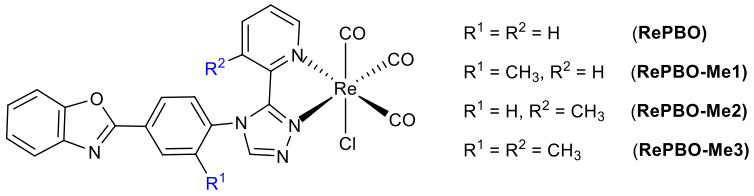

Scheme 1 Chemical structure of the tricarbonylrhenium(I) complexes.

2. Experimental section

2.1. General methods and synthesis

All purchased chemicals were of the highest purity commercially available and used without further purification. Analytical grade solvents were used as received. Unless otherwise noted, all experiments were carried out under a nitrogen atmosphere. Reactions were monitored by TLC on silica gel Alugram® Xtra SIL G/UV$_{254}$ or by TLC on aluminum oxide Alugram® ALOX N/UV$_{254}$. Column chromatography was performed on Machery-Nagel silica gel or alumina grade IV.

NMR, mass and infrared spectra were obtained in the relevant 'Services communs de l'Institut de Chimie de Toulouse, Université de Toulouse III-Paul-Sabatier'. ^{1}H- and ^{13}C-NMR spectra were recorded on Bruker Avance 300 MHz, 400 MHz and 500 MHz spectrometers. Attributions of the signals were made using 2D NMR data (HSQC and HMBC). The numbering of protons and carbon atoms, as well as the whole set of spectra are given in Fig. S1–10. Signals are described as follow: s, singlet; d, doublet; t, triplet; m, multiplet. App = Apparent; * = The multiplicity of the signal is more complex as it is part of an AAXX system, ** = Split signal, corresponding to two conformers.

High resolution mass spectrometry (HRMS) data were recorded on a Xevo G2 QTOF (Waters) instrument. Fourier transform infrared spectra were obtained on a Nexus Thermonicolet apparatus with DTGS as the detector. Melting points (Mp) were obtained on a Buchi apparatus and are uncorrected. Measurements above 200°C were not possible with this apparatus.

2-Pyridinecarboxylic acid hydrazide (**5**) was purchased from TCI. 2-(4-Aminophenyl)benzoxazole (**1**) and *N*,*N*-dimethyl-*N'*-picolinoylformohydrazonamide (HDA) (**6**) were prepared as previously described [15].

2-(4-Amino-3-tolyl)benzoxazole (2). A mixture of 2-aminophenol (0.5 g, 4.58 mmol), 4-amino-3-methylbenzoic acid (0.7 g, 4.58 mmol) and polyphosphoric acid (8.9 g) was heated at 205°C for 4h under stirring. After cooling down, distilled water (200 mL) was added to the mixture and a saturated aqueous solution of $NaHCO_3$ was slowly poured into the solution until no bubbling was detected. After filtration, washing with water and drying, the solid obtained was sublimated at 240°C under vacuum. The desired compound was obtained as a yellow solid (740 mg, yield: 72%).
^{1}H NMR (300 MHz, chloroform-*d*): δ (ppm) = 8.02 (dd, *J* = 2.0, 0.9 Hz, 1H), 7.97 (ddd, *J* = 8.2, 2.1, 0.6 Hz, 1H), 7.78–7.69 (m, 1H), 7.60–7.52 (m, 1H), 7.36–7.30 (m, 2H), 6.79 (d, *J* = 8.3 Hz, 1H), 2.29

(s, CH_3, 3H). ^{13}C NMR (75 MHz, chloroform-*d*): δ (ppm) = 164.0, 150.5, 148.0, 142.3, 130.1, 127.10, 124.2, 124.1, 122.0, 119.2, 116.8, 114.5, 110.2, 17.2.

3-Methylpyridine-2-methylcarboxylate (3). According to a procedure described in the literature [19], 3-methylpyridine-2-carboxylic acid (0.5 g, 3.7 mmol) was dissolved in methanol with some drops of sulfuric acid, the mixture was refluxed for 16 h, and then methanol was evaporated. The resulting crude product was dissolved in dichloromethane and neutralized with $NaHCO_3$. After addition of 10 mL of water, the organic phase was extracted with dichloromethane, washed with water, and the solvent was evaporated, giving a colorless oil (445 mg) (Yield = 81%).
^{1}H NMR (300 MHz, chloroform-*d*): δ (ppm) = 8.55 (ddd, *J* = 4.6, 1.7, 0.6 Hz, 1H), 7.61 (ddd, *J* = 7.8, 1.7, 0.8 Hz, 1H), 7.34 (dd, H_2, *J* = 7.8, 4.7 Hz, 1H), 3.98 (s, O$C\underline{H}_3$, 3H), 2.60 (s, $C\underline{H}_3$, 3H).

3-Methylpyridine-2-carbohydrazide (4). As described in the literature [20], **3** (0.36 g, 2.38 mmol) and hydrazine (0.31 g, 9.6 mmol) diluted in methanol (10 mL) were heated to reflux for 16 h. Methanol was evaporated. The crude product was purified on a silica column using dichloromethane as eluent, resulting in 349 mg of a white solid (Yield = 97%).
^{1}H NMR (300 MHz, chloroform-*d*): δ (ppm) = 9.03 (s, 1H), 8.36 (ddd, *J* = 4.6, 1.7, 0.7 Hz, 1H), 7.57 (ddd, *J* = 7.8, 1.7, 0.8 Hz, 1H), 7.29 (dd, *J* = 7.8, 4.6 Hz, 1H), 2.70 (s, 3H).

***N*,*N*-Dimethyl-*N'*-3-methylpicolinoylformohydrazonamide (MHDA) (7).** Compound **4** (0.102 g, 0.67 mmol) and *N*,*N*-dimethylformamide dimethylacetal (0.105 g, 0.8 mmol) dissolved in 5 mL dichloromethane were stirred at 50°C for 16 h. The solvent was evaporated and the crude product was purified by column chromatography on silica, using a mixture of dichloromethane/methanol as eluent (gradient from 99:1 to 98:2 v/v). A yellow solid (94.3 mg) was obtained (Yield = 68%).
^{1}H NMR (300 MHz, chloroform-*d*): δ (ppm) = 10.07 (s, 1H), 8.11 (ddd, *J* = 4.6, 1.7, 0.7 Hz, 1H), 7.80 (s, 1H), 7.36 (ddd, *J* = 7.8, 1.7, 0.7 Hz, 1H), 7.06 (dd, *J* = 7.8, 4.6 Hz, 1H), 2.74 (s, 6H), 2.52 (s, 3H). ^{13}C NMR (75 MHz, acetonitrile-d_3): δ (ppm) = 161.4, 155.4, 147.3, 144.8, 140.1, 134.5, 124.7, 36.0, 19.7.

2-(3-Methylpyridin-2-yl)-1,3,4-oxadiazole (8). Compound **4** (515 mg, 3.4 mmol) and triethyl orthoformate (4 mL) were heated for 16 h at 150°C. Triethyl orthoformate was removed and the residue was stirred at 200°C for 2 h. The crude product was purified by chromatography on silica using a mixture of dichloromethane/ethylacetate 90:10 v/v as eluent. A white solid (350 mg) was obtained (Yield = 64 %).
^{1}H NMR (300 MHz, chloroform-*d*): δ (ppm) = 8.63 (ddd, *J* = 4.1, 1.7, 0.9 Hz, 1H), 8.56 (s, 1H), 7.73 (dd, *J* = 7.9, 0.8 Hz, 1H), 7.38 (dd, *J* = 7.8, 4.7 Hz, 1H), 2.80 (s, 3H). ^{13}C NMR (75 MHz, chloroform-*d*): δ (ppm) = 163.8, 152.9, 147.4, 141.6, 139.9, 135.5, 125.4, 20.8.

2-(3-Methyl-4-(3-(pyridin-2-yl)-4H-1,2,4-triazol-4-yl)phenyl)benzoxazole (L1). Compounds **2** (244 mg, 1.09 mmol) and **6** (272 mg, 1.41 mmol) were dissolved in 5 mL acetonitrile in the presence of acetic acid (622 µL 10.88 mmol) and heated overnight at 110°C. The crude product was purified by column chromatography using ethylacetate as eluent, and the resulting compound was washed with diethylether. A white solid (96 mg) was obtained (Yield = 25%).
^{1}H NMR (300 MHz, chloroform-*d*): δ (ppm) = 8.38–8.24 (m, H_{11}, H_{15}, H_{17}, H_{23}, 4H), 8.19 (dd, H_{26}, *J* = 8.3, 2.0 Hz, 1H), 7.87–7.76 (m, H_4, H_{25}, 2H), 7.70–7.59 (m, H_7, 1H), 7.47–7.34 (m, H_5, H_6, H_{14}, 3H), 7.24 (ddd, H_{24}, *J* = 7.6, 4.8, 1.2 Hz, 1H), 2.13 (s, H_{27}, 3H). ^{13}C NMR (75 MHz, chloroform-*d*): δ (ppm) = 161.9 (C_2), 152.3 (C_{20}), 150.8 (C_9), 149.0 (C_{23}), 146.5 (C_{21}), 145.2 (C_{17}), 141.9 (C_8), 137.8 (C_{13}), 136.8 (C_{25}), 136.2 (C_{14}), 129.8 (C_{15}), 128.1 (C_{10}), 127.6 (C_{12}), 125.8 (C_{26}), 125.6 (C_5), 124.8 (C_6), 124.2 (C_{24}), 123.1 (C_{11}), 120.2 (C_4), 110.7 (C_7), 17.8 (C_{27}). ESI$^+$ HRMS: *m/z* 354.1352 ([M+H]$^+$) calcd for $C_{21}H_{16}N_5O$, 354.1355.

2-(4-(3-(3-Methyl-pyridin-2-yl)-4H-1,2,4-triazol-4-yl)phenyl)benzoxazole (L2). A mixture of **1** (262 mg, 1.24 mmol), **8** (201 mg, 1.24 mmol) and *p*-toluene sulfonic acid (24 mg, 0.12 mmol) in xylene (2 mL) was heated in 150°C for 20 h. The crude product was purified by column chromatography on silica

using ethylacetate as eluent, and then on alumina using dichloromethane/methanol 95:5 as eluent. A white solid (220 mg) was obtained (Yield = 50 %).
^{1}H NMR (300 MHz, chloroform-*d*): δ (ppm) = 8.49 (s, H_{17}, 1H), 8.31–8.22 (m, H_{11}, H_{15}, H_{23}, 3H), 7.82–7.73 (m, H_4, 1H), 7.65 (ddd, H_{25}, *J* = 7.8, 1.6, 0.8 Hz, 1H), 7.62–7.55 (m, H_7, 1H), 7.43–7.36 (m, H_5, H_6, 2H), 7.33 (app. d*, H_{12}, H_{14}, *J* = 6.8 Hz, 2H), 7.22 (dd, H_{24}, *J* = 7.8, 4.7 Hz, 1H), 2.55 (s, H_{27}, 3H). ^{13}C NMR (75 MHz, chloroform-*d*): δ (ppm) = 161.5 (C_2), 151.7 (C_{20}), 150.8 (C_8), 146.7 (C_{23}), 145.0 (C_{21}), 143.8 (C_{17}), 143.7 (C_{10}), 141.9 (C_9), 138.9 (C_{25}),137.3 (C_{13}), 135.0 (C_{26}), 128.6 (C_{11}, C_{15}), 125.6 (C_{12}, C_{14}), 125.5 (C_5, C_6), 124.2 (C_{24}), 120.2 (C_4), 110.7 (C_7), 19.4 (C_{27}). ESI$^+$ HRMS: *m/z* 354.1354 ([M+H]$^+$) calcd for $C_{21}H_{16}N_5O$, 354.1355.

2-(3-Methyl-4-(3-(3-methyl-pyridin-2-yl)-4H-1,2,4-triazol-4-yl)phenyl)benzoxazole (L3). 2-(4-Amino-3-tolyl)benzoxazole (**2**) (200 mg, 0.89 mmol), **7** (276 mg, 1.34 mmol), acetic acid (200 µL, 4.46 mmol) and trifluoroacetic acid (276 µL, 3.57 mmol) in 10 mL acetonitrile were heated in 120°C for 24 h. The crude product was purified by column chromatography on silica using ethylacetate as eluent, then on alumina using as eluent a mixture of dichloromethane/methanol with a gradient passing from 100:0 to 98:2 v/v. A white solid (72 mg) was obtained (Yield = 22 %).
^{1}H NMR (300 MHz, chloroform-*d*): δ (ppm) = 8.35 (s, H_{17}, 1H), 8.20 (dd, H_{15}, *J* = 2.0, 0.8 Hz, 1H), 8.18–8.09 (m, H_{11}, H_{23}, 2H), 7.87–7.76 (m, H_4, 1H), 7.62 (m, H_7, H_{25}, 2H), 7.47–7.38 (m, H_5, H_6 2H), 7.36 (d, H_{14}, *J* = 8.2 Hz, 1H), 7.14 (dd, H_{24}, *J* = 7.8, 4.7 Hz, 1H), 2.71 (s, H_{28}, 3H), 2.13 (s, H_{27}, 3H). ^{13}C NMR (75 MHz, chloroform-*d*): δ (ppm) = 161.8 (C_2), 152.3 (C_{20}), 150.8 (C_8), 146.4 (C_{23}), 144.8 (C_{21}), 144.1 (C_{17}), 141.9 (C_9), 138.9 (C_{25}), 137.2 (C_{13}), 135.8 (C_{14}), 134.5 (C_{26}), 129.8 (C_{15}), 128.3 (C_{10}), 127.9 (C_{12}), 125.7 (C_{11}), 125.5 (C_5), 124.8 (C_6), 123.8 (C_{24}), 120.1 (C_4), 110.6 (C_7), 20.0 (C_{28}), 17.6 (C_{27}). ESI$^+$ HRMS: *m/z* 368.1516 ([M+H]$^+$ calcd for $C_{22}H_{18}N_5O$, 368.1511.

General procedure for the preparation of tricarbonylrhenium(I) complexes
A mixture of the ligand and [Re(CO)$_5$Cl] (1.05–1.1 eq.) in methanol was stirred for 16 h at 65°C. The reaction mixture was cooled to room temperature and the yellow precipitate was collected by filtration, washed with methanol and dried *in vacuo*. The expected product was pure enough to be used without further purification.

Complex [Re(CO)$_3$(L1)Cl] (RePBO-Me1). Following the general procedure, 97 mg (0.27 mmol) of **L1** and 104.4 mg (0.29 mmol) of [Re(CO)$_5$Cl] afforded complex **RePBO-Me1** (167 mg) as a yellow solid (Yield 94%). ^{1}H NMR (500 MHz, chloroform-*d*): δ (ppm) = 9.17–9.13 (m, H_{23}, $H_{23'}$, 1H), 8.50–8.37 (m, H_{11}, $H_{11'}$, H_{15}, $H_{15'}$, 2H), 8.36 (s, $H_{17'}$, 0.35H**), 8.35 (s, H_{17}, 0.65H**), 7.88–7.83 (m, H_4, $H_{4'}$, 1H), 7.82–7.77 (m, H_{25}, $H_{25'}$, 1H), 7.70–7.64 (m, H_7, $H_{7'}$, H_{14}, $H_{14'}$, 2H), 7.55–7.51 (m, H_{24}, $H_{24'}$, 1H), 7.49 – 7.43 (m, H_5, $H_{5'}$, H_6, $H_{6'}$, 2H), 6.94 (dt, H_{26}, $H_{26'}$, *J* = 8.0, 1.1 Hz, 1H), 2.27 (s, $H_{27'}$, 1H**), 2.19 (s, H_{27}, 2H**). ^{13}C NMR (125 MHz, chloroform-*d*): δ (ppm) = 197.18 (CO), 197.15 (CO'), 195.19 (CO), 194.97 (CO'), 188.29 (CO), 188.08 (CO'), 160.57 (C_2), 160.50 ($C_{2'}$), 154.96 ($C_{23'}$), 154.89 (C_{23}), 154.73 (C_{20}), 154.51 ($C_{20'}$), 151.0 (C_9-$C_{9'}$), 145.73 (C_{17}), 145.47 ($C_{17'}$), 144.89 (C_{21}), 144.58 ($C_{21'}$), 141.79 (C_8), 141.77 ($C_{8'}$), 139.11 (C_{25}, $C_{25'}$), 137.35 (C_{12}), 135.89 ($C_{12'}$), 133.24 (C_{13}), 133.14 ($C_{13'}$), 131.41 (C_{11}), 131.22 ($C_{11'}$), 131.19 (C_{10}), 131.17 ($C_{10'}$), 128.38 ($C_{14'}$), 127.81 ($C_{24'}$), 127.69 (C_{24}), 127.54 ($C_{15'}$), 127.50 (C_{14}), 127.27 (C_{15}), 126.39 ($C_{5'}$), 126.38 (C_5), 125.33 (C_6, $C_{6'}$), 121.98 ($C_{26'}$), 121.81 (C_{26}), 120.63 (C_4, $C_{4'}$), 110.96 ($C_{7'}$), 110.93 (C_7), 17.72 (C_{27}), 17.60 ($C_{27'}$). ESI$^+$ HRMS: *m/z* 682.0263 ([M + Na]$^+$) calcd for $C_{24}H_{15}N_5O_4ClNa^{187}Re$, 682.0268. IR (KBr pellet): $\nu_{(CO)}$ = 2018, 1916 and 1890 cm^{-1}. Anal. calcd (%) for $C_{24}H_{15}N_5O_4ClRe$: C 43.74, H 2.29, N 10.63; found: C 43.88, H 2.29, N 9.95.

Complex [Re(CO)$_3$(L2)Cl] (RePBO-Me2). Following the general procedure, 41 mg (0.11 mmol) of **L2** and 44 mg (0.12 mmol) of [Re(CO)$_5$Cl] in 5 mL methanol afforded complex **RePBO-Me2** (63 mg) as a yellow solid (Yield 87%). ^{1}H NMR (500 MHz, chloroform-*d*): δ (ppm) = 9.09–9.04 (m, H_{23}, 1H), 8.57–8.38 (m, H_{17}, H_{11}, H_{15}, 3H), 7.84–7.81 (m, H_4,1H), 7.74 (ddd, H_{25}, *J* = 8.0, 1.5, 0.8 Hz, 1H), 7.67–7.62 (m, H_7,1H), 7.61–7.54 (m, H_{12}, H_{14}, 2H), 7.51 (dd, H_{24}, *J* = 8.0, 5.3 Hz, 1H), 7.48–7.40 (m, H_5, H_6, 2H), 1.80 (s, H_{27}, 3H). ^{13}C NMR (125 MHz, chloroform-*d*): δ (ppm) = 197.2 (CO), 195.4 (CO), 189.0 (CO), 160.4 (C_2), 157.6 (C_{20}), 152.7 (C_{23}), 150.9 (C_9), 147.2 (C_{17}), 144.0 (C_{21}), 142.6 (C_{25}), 141.8 (C_8), 136.2 (C_{13}), 134.8 (C_{26}), 130.0 (C_{10}), 129.9 (C_{11}, C_{15}), 127.3 (C_{24}), 126.3 (C_5), 125.6 (C_{12}, C_{14}), 125.43 (C_6), 120.6 (C_4), 110.9 (C_7), 20.5 (C_{27}). ESI$^+$ HRMS: *m/z* 682.0272 ([M + Na]$^+$) calcd for

$C_{24}H_{15}N_5O_4ClNa^{187}Re$, 682.0268. IR (KBr pellet): $\nu_{(CO)}$ = 2018, 1920 and 1873 cm^{-1}. Anal. calcd (%) for $C_{24}H_{15}N_5O_4ClRe$: C 43.74, H 2.29, N 10.63; found: C 42.58, H 1.84, N 10.31.

Complex [Re(CO)$_3$(L3)Cl], (RePBO-Me3). Following the general procedure, 40 mg (0.109 mmol) of **L3** and 51 mg (0.14 mmol) of [Re(CO)$_5$Cl] afforded complex **RePBO-Me3** (52 mg) as a yellow solid (Yield 72%). ^{1}H NMR (500 MHz, tetrachloroethane-d_2): δ(ppm) = 9.10 (dd, $H_{23\text{-}23'}$, J = 5.3, 1.4 Hz, 1H), 8.50–8.46 (m, H_{17}, $H_{17'}$, $H_{11'}$, 1.5H**), 8.42–8.37 (m, $H_{15'}$, H_{11}, 1H**), 8.23 (dd, H_{15}, J = 8.4, 2.1 Hz, 0.5H**), 7.91–7.87 (m, H_4, $H_{4'}$, 1H), 7.82–7.79 (m, H_{25}, $H_{25'}$, 1H), 7.77–7.73 (m, H_7, $H_{7'}$, 1H), 7.69–7.62 (m, $H_{14'}$, H_{24}, $H_{24'}$, 1.5H**), 7.54–7.45 (m, H_5, $H_{5'}$, H_6, $H_{6'}$, 2H), 7.32 (d, H_{14}, J = 8.2 Hz, 0.5H**), 2.49 (s, H_{27}, 1.5H**), 2.15 (s, $H_{27'}$, 1.5H**), 1.77 (s, $H_{28'}$, 1.5H**), 1.74 (s, H_{28}, 1.5H**). ^{13}C NMR (125 MHz, tetrachloroethane-d_2): δ (ppm) = 197.74 (CO), 197.70 (CO'), 196.16 (CO), 196.04 (CO'), 189.19 (CO), 189.01 (CO'), 160.7 (C_2, $C_{2'}$), 158.2 (C_{20}), 157.5 ($C_{20'}$), 152.84 (C_{23}), 152.79 ($C_{23'}$), 151.0 (C_9, $C_{9'}$), 147.1 (C_{17}, $C_{17'}$), 144.2 ($C_{21'}$), 143.9 (C_{21}), 143.1 ($C_{25'}$), 143.0 (C_{25}), 141.80 ($C_{8'}$), 141.79 (C_8), 136.2 (C_{13}), 135.6 ($C_{13'}$), 135.4 ($C_{12'}$), 135.1 (C_{26}), 134.8 ($C_{26'}$), 134.0 (C_{12}), 131.5 (C_{11}), 131.3 ($C_{11'}$), 130.2 ($C_{10'}$), 130.1(C_{10}), 127.7 (C_{14}), 127.65 (C_{24}), 127.60 ($C_{24'}$), 127.44 (C_{15}), 127.29 ($C_{14'}$), 127.24 ($C_{15'}$), 126.46 ($C_{5'}$), 126.45 C_5), 125.41 ($C_{6'}$), 125.40 (C_6), 120.67 ($C_{4'}$), 120.64 (C_4), 111.2 (C_7, $C_{7'}$), 20.9 ($C_{28'}$), 20.2 (C_{28}), 18.5 ($C_{27'}$), 17.96 (C_{27}).
^{1}H NMR (500 MHz, chloroform-d): δ(ppm) = 9.10–9.05 (m, H_{23}, $H_{23'}$, 1H), 8.43–8.41 (m, H_{17}, $H_{15'}$, 1H**), 8.39 (s, $H_{17'}$, 0.5H**), 8.36–8.29 (m, $H_{11'}$, H_{15}, 1H**), 8.17 (dd, H_{11}, J = 8.4, 2.6 Hz, 0.5H**), 7.84–7.80 (m, H_4, $H_{4'}$, 1H), 7.75–7.68 (m, H_{25}, $H_{25'}$, 1H), 7.66–7.61 (m, H_7, $H_{7'}$, 1H), 7.60 (d, $H_{14'}$, J = 8.1 Hz , 0.5H**), 7.50–7.48 (m, H_{24}, $H_{24'}$, 1H), 7.47–7.40 (m, H_5, $H_{5'}$, H_6, $H_{6'}$, 2H), 7.34 (d, H_{14}, J = 8.3 Hz, 0.5H**), 2.48 (s, H_{27}, 1.5H**), 2.13 (s, $H_{27'}$, 1.5H**), 1.76 (s, $H_{28'}$, 1.5H**), 1.72 (s, H_{28}, 1.5H**). ESI$^+$ HRMS: *m/z* 696.0422 ([M + Na]$^+$) calcd for $C_{25}H_{17}N_5O_4ClNa^{187}Re$, 696.0424. IR (KBr pellet): $\nu_{(CO)}$ = 2021, 1913 and 1881 cm^{-1}. Anal. calcd (%) for $C_{25}H_{17}N_5O_4ClRe$: C 44.41, H 2.98, N 10.36; found: C 44.01, H 2.16, N 10.34.

2.2. X-ray crystallography

Crystal data were collected at 193K using MoKα radiation (wavelength = 0.71073 Å) on a Bruker AXS Quazar APEX II diffractometer using a 30 W air-cooled microfocus source (ImS) with focusing multilayer optics (**Re-PBO-Me2(a)**) and on a Bruker-AXS D8-Venture equipped with a Photon III-C14 detector (**Re-PBO-Me1**, **Re-PBO-Me2(b)** and **Re-PBO-Me3**). Phi- and omega-scans were used. Space group was determined on the basis of systematic absences and intensity statistics. Semi-empirical absorption correction was employed [21]. The structures were solved using an intrinsic phasing method (ShelXT) [22]. All non-hydrogen atoms were refined anisotropically using the least-square method on F^2 [23]. Hydrogen atoms were refined isotropically at calculated positions using a riding model with their isotropic displacement parameters constrained to be equal to 1.5 times the equivalent isotropic displacement parameters of their pivot atoms for terminal sp3 carbon and 1.2 times for all other carbon atoms. Some parts of the structures were found to be disordered, especially the solvents molecules. Several restraints (SAME, SADI, SIMU, DELU, ISOR, DFIX) and equal xyz and U_{ij} constraints EXYZ and EADP (for **Re-PBO-Me2(b)**) were applied to refine some moieties of the molecules and to avoid the collapse of the structures during the least-squares refinement by the large anisotropic displacement parameters. Selected crystallographic data are collected in Tables 1, S1 and S2.

	RePBO-Me1	**RePBO-Me2(a)**	**RePBO-Me2(b)**	**RePBO-Me3**
Empirical formula	$C_{24}H_{15}N_5O_4ClRe \cdot C_4H_{10}O$	$C_{24}H_{15}N_5O_4ClRe$	$C_{24}H_{15}N_5O_4ClRe \cdot (CH_2Cl_2)_{3.5}$	$C_{25}H_{17}N_5O_4ClRe \cdot (CH_4O)_{0.5}$
Formula weight	733.18	659.06	956.3	689.11
Crystal system	Triclinic	Monoclinic	Triclinic	Orthorhombic
Space group	$P\bar{1}$	$P2_1/n$	$P\bar{1}$	$Pbcn$
Unit cell dimensions				
***a* (Å)**	7.9159(4)	12.1419(12)	10.1844(4)	19.1647(12)
***b* (Å)**	14.0960(6)	18.3549(16)	12.4230(5)	12.4517(8)
***c* (Å)**	14.2939(7)	20.382(2)	15.2607(6)	20.2131(11)
***α* (°)**	116.7249(16)	90	105.3059(16)	90
***β* (°)**	100.6337(19)	91.195(3)	104.1318(15)	90
***γ* (°)**	93.6070(17)	90	92.3734(16)	90

Volume (Å^3)	1380.63(12)	4541.5(7)	1794.35(12)	4823.5(5)
Z	2	8	2	8
Density (calculated) (Mg/m^3)	1.764	1.928	1.770	1.898
Crystal size (mm^3)	0.250 × 0.050 × 0.030	0.120 × 0.030 × 0.020	0.130 × 0.150 × 0.200	0.140 × 0.060 × 0.050
Reflections collected	36786	73347	54016	184788
Independent reflections	6857	8016	8824	5996
R_{int}	0.0459	0.2440	0.0242	0.1680
Restraints/parameters	129 / 408	66/633	338 / 564	8 / 347
Final R1 index I>2σ(I)	0.0266	0.0640	0.0212	0.0304
wR2 (all data)	0.0629	0.1422	0.0582	0.0638
Largest diff. peak and hole (e Å^{-3})	0.836 and -0.749	2.748 and -1.542	0.816 and -0.762	0.842 and -0.663
CCDC	2253587	2253588	2253589	2253590

Table 1. Selected crystallographic data of complexes **RePBO-Me1**, **RePBO-Me2** (**a** and **b** forms) and **RePBO-Me3**.

2.3. Electrochemistry

The electrochemical properties of the new compounds were determined by cyclic voltammetry (CV) and Osteryoung square wave voltammetry (OSWV) in dichloromethane (DCM). The solutions used during the electrochemical studies were typically 1×10^{-3} M in complex, and 0.1 M in supporting electrolyte. The supporting electrolyte [*n*Bu$_4$N][BF$_4$] (Fluka, 99% electrochemical grade) was used as received and simply degassed under Ar. DCM was dried using an MB SPS-800 solvent purification system just prior to use. The measurements were carried out with an Autolab PGSTAT100 potentiostat controlled by GPES 4.09 software. Experiments were performed at room temperature (r.t.) in a homemade airtight three-electrode cell connected to a vacuum/Ar line. The reference electrode consisted of a saturated calomel electrode (SCE) separated from the solution by a bridge compartment. The counter electrode was a Pt wire of *ca*. 1 cm^2 apparent surface. The working electrode was a Pt microdisk (0.5 mm diameter). Before each measurement, the solutions were degassed by bubbling Ar and the working electrode was polished with a polishing machine (Presi P230). Under these experimental conditions, Fc^+/Fc was observed at +0.55 ± 0.01 V *vs*. SCE. OSWVs were obtained using an amplitude of 20 mV, a frequency of 20 Hz, and a step potential of 5 mV.

2.4. Spectroscopy

Spectroscopic measurements in air-equilibrated solutions were conducted at 20°C in a temperature-controlled cell. UV-visible absorption spectra and fluorescence spectra in solutions were measured with a Xenius SAFAS spectrofluorometer using cells of 1 cm optical pathway. All fluorescence spectra in solution were corrected. The fluorescence quantum yields in solution (Φ_F) were determined using the classical formula: $\Phi_{Fx} = (A_s \times F_x \times n_x^2 \times \Phi_{Fs})/(A_x \times F_s \times n_s^2)$ where A is the absorbance at the excitation wavelength, F the area under the fluorescence curve and n the refractive index. Subscripts s and x refer to the standard and to the sample of unknown quantum yield, respectively. Coumarin 153 (Φ_F = 0.53) in ethanol was used as the standard [24]. The absorbance of the solutions was equal or below 0.06 at the excitation wavelength. The error on the quantum yield values is estimated to be about 10%.

To investigate the aggregation-induced emission (AIE) effect, 30 µL of a concentrated acetonitrile solution of the three complexes were injected into 2970 µL of various acetonitrile/water mixtures. The samples were left to stand at room temperature (25°C) under mechanical stirring for 3h. They were excited at 350 nm, which is quasi-isosbestic point for samples up to 70% water. The baseline deviation due to scattering was not taken into account.

Solid state photoluminescence spectra were recorded using a Fluorolog spectrofluorometer from HORIBA Scientific, and they are corrected. The photoluminescence quantum yields (PLQY) were recorded on the Xenius SAFAS spectrofluorometer equipped with an integrating sphere. Solid samples were deposited on a metal holder. The absolute PLQY values (Φ_P) were determined by a method based

on the one developed by de Mello *et al.* [25], as described elsewhere [15]. The error was estimated to be about 20%.

Emission decay curves of dilute DCM solutions (Abs at λ_{ex}< 0.1) were recorded using the time-correlated single-photon counting method (TCSPC) on a Fluorolog 3-2(iHR320) spectrofluorimeter equipped with a nanoled-370 (λ_{ex} = 371 nm). Emitted photons were detected at 90° through a monochromator by means of a Hamamatsu R928 photomultiplier. Emission was recorded near the maximum with a bandpass of 10-15 nm. The instrumental response was recorded directly on the sample at 371 nm before each decay curve. All analyzes were recorded using the Datastation v2.7 software. The decay curves were analyzed with reconvolution and global non-linear least-squares minimization method using DAS6 v6.8 software.

Decay curves of solid samples were measured using an LP920-K spectrometer equipped with a monochromator with 300 mm focus, and a photomultiplier (Hamamatsu R928). Quartz sample holders from Starna, with 0.2 mm between both slides, were used. The samples were excited (420 nm) by an OPO pumped by an oscillating Nd:YAG nanosecond laser (7-8 ns) with a repetition rate of 10 Hz at its third harmonic generation (355 nm). The instrumental response function was recorded with each set of decay curves. The data were analyzed with reconvolution using the L900 software.

Fluorescence microscopy was performed with a Leitz Laborlux D fluorescence microscope equipped with an Andor Luca camera (λ_{ex} ~ 450−490 nm, λ_{em} > 500 nm).

2.5. Computational details

The ORCA software was employed for all calculations with the aid of the Gebedit visualization program [26]. Density functional theory (DFT) and time-dependent DFT (TD-DFT) calculations were performed with the PBE0 functional [27]. The ground state (S_0), the first excited state (S_1) and the lowest triplet state (T_1) geometries of compounds were fully optimized with the DFT method using the Perdew-Burke-Ernzerhof PBE0 functional without symmetry constraints [28]. In all calculations, the "double-ζ" quality basis set LANL2DZ with Hay and Wadt's relative effective core potential ECP (outer-core [($5s^2 5p^6$)] electrons and the ($5d^6$) valence electrons) [29, 30] was employed for the Re atom. The solvent effect (dichloromethane, ε = 9.08) was simulated using the Conductor-like Polarizable Continuum Model (CPCM) [31, 32]. The vibrational frequencies calculations were performed using the optimized structural parameters of compounds, to confirm that each optimized structure represents a local minimum on the potential energy surface and all eigenvalues are non-negative. On the basis of the optimized ground and excited state geometries, the UV-vis absorption and emission spectral properties were calculated by the TD-DFT method at the PBE0/LANL2DZ level. The emission has been calculated by DFT with the difference of energy between the optimized triplet state and the singlet state at the same geometry.

3. Results and discussion

3.1. Synthesis

The procedure used to synthesize the methylated complexes, described in Scheme 2, is a variant of that previously used for **RePBO** [15]. The details of synthesis and the chemical characterization of the compounds are given in the Experimental Section. In brief, 2-amino-phenol was condensed with 4-aminobenzoic acid or 4-amino-3-methylbenzoic acid in the presence of polyphosphoric acid to give the corresponding 4'-amino-PBO derivatives (**1** or **2**). *N*,*N*-Dimethyl-*N'*-picolinoylformohydrazonamide (HDA) (**6**) [15] was obtained from the commercially-available pyridine carbohydrazide (**5**) [33], and *N*,*N*-dimethyl-*N'*-3-methylpicolinoylformohydrazonamide (MHDA) (**7**) was obtained from the specially prepared 3-methylpyridine-2-carbohydrazide (**4**) [20]. The 4'-amino-PBO derivative **2** was then reacted with (**6**) and (**7**) to give the corresponding ligands **L1** and **L3** with an overall yield around 25%. Side reactions of the hydrazonamide derivative were responsible for this modest yield, so an alternative strategy was developed for the synthesis of **L2**. 3-Methyl-2-(1,3,4-oxadiazol-2 yl) pyridine (**8**) was first synthesized in one step procedure by heating 3-methylpyridine-2-carbohydrazide (**4**) in

triethyl orthoformate at 150°C, and then at 200°C after elimination of triethyl orthoformate [34]. Then, the 4'-amino-PBO derivative **1** was reacted with **8** in the presence of catalytic *p*-TsOH in refluxing xylene, to give **L2** in 50% yield after purification [35]. Although this second route provides the desired compound in higher yield, the synthesis of **L3** was not optimized using this pathway. The ligands were then reacted with $[Re(CO)_5Cl]$ in refluxing methanol to afford the corresponding tricarbonylrhenium(I) complexes in good yields (94%, 87% and 72%, for **RePBO-Me1**, **RePBO-Me2** and **RePBO-Me3**, respectively). The complexes were characterized by ^{1}H and ^{13}C NMR spectroscopy (Fig. S2–10), high resolution mass spectrometry, infrared spectroscopy and elemental microanalysis.

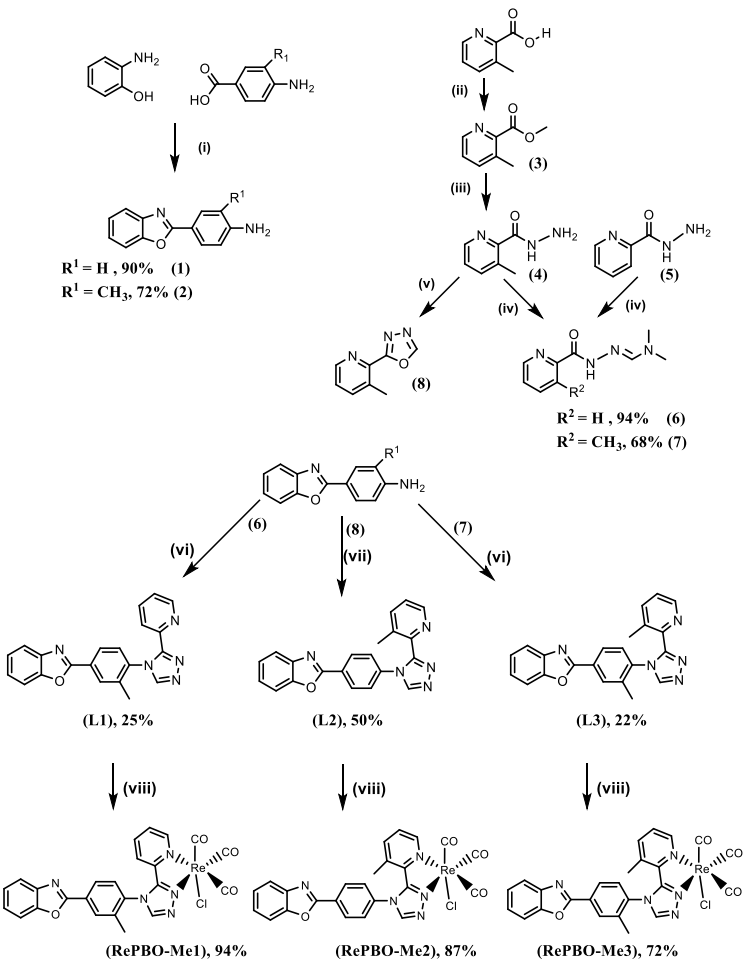

Scheme 2. Synthetic procedure for complexes **RePBO-Me1**, **RePBO-Me2** and **RePBO-Me3**: (i) polyphosphoric acid, 205 ºC, 4 h; (ii) sulfuric acid, MeOH, reflux, 16 h; (iii) hydrazine, MeOH, 80°C, 16 h; (iv) *N*,*N*-dimethylformamide dimethylacetal, dichloromethane, 50°C, 16 h; (v) triethyl orthoformate, 150°C, 16 h, and then 200°C, 2 h after removing the solvent; (vi) **L1**: acetic acid, CH_3CN, 110°C, 16 h, **L3**: acetic acid, trifluoroacetic acid, CH_3CN, 120°C, 24 h; (vii) **L2**: Xylene, *p*-toluene sulfonic acid, 150°C, 20 h; (viii) $[Re(CO)_5Cl]$, MeOH, 65ºC, 16 h.

3.2. Crystal structures

Crystals of **RePBO-Me1** and **RePBO-Me3** were obtained by slow evaporation at room temperature of saturated solutions of these compounds in chloroform/diethylether mixture and methanol, respectively. Crystals of **RePBO-Me2** were quite difficult to grow, so that crystallization was performed at -80°C in dichloromethane. The X-ray structures were determined for the three compounds. The corresponding molecular views with the complete numbering of the atoms, and the characteristic

data (distances and angles) are given in Tables S1 and S2, in comparison with those of the parent compound **RePBO**. Selected crystallographic data are collected in the experimental section (Table 1)

Unsurprisingly, the coordination sphere of the three methylated complexes is almost the same. It exhibits a slightly-distorted octahedral geometry. The rhenium atom is coordinated to three carbonyl groups in a *fac* configuration, two nitrogen atoms of the pyta ligand and one chlorine atom. Distances and angles are close to those of **RePBO** [15] and differ little from one compound to another. In contrast, strong differences appear when considering the geometry of the organic moiety and the intermolecular arrangement.

The asymmetric unit of **RePBO-Me1** consists of one molecule of complex and one molecule of diethylether crystallizing in the $P\ \bar{1}$ space group. The phenyl-triazole angle (α) of the complex is approximately 73°, and the pyta moiety is almost flat with a pyridyl-triazole angle (β) of 3.6° (Fig. 1). The intermolecular arrangement shows that the PBO moieties are all situated on parallel planes, with their long axis oriented along two opposite directions. There is no overlap between PBO moieties due to the lateral and longitudinal shifts of neighboring molecules. No overlap was observed either between the triazole rings belonging to two neighboring molecules, which are parallel with a centroid-to-centroid distance of about 3.7 Å, but significantly shifted with respect to each other. Some intermolecular short-distance contacts can also be noticed, for example between the nitrogen atom (N5) of benzoxazole and the carbon atom (C10) of triazole (3.2 Å), as well as between the chlorine atom and one hydrogen atom of the pyridyl ring.

The crystallization of **RePBO-Me2** led to very small needles of pure compound (**RePBO-Me2(a)**), as well as platelets corresponding to a solvate made of seven dichloromethane molecules for two molecules of complex (**RePBO-Me2(b)**). In both types of crystals, the molecules have almost the same geometry: the phenyl-triazole angle (α) is as small as ~57°, and the pyta moiety is twisted with angle β from 20° to 24°. However, a marked difference is that if looking perpendicular to the plane of the pyta moiety, it can be seen that the chloride ligand faces the PBO unit in **RePBO-Me2(a)**, while this position is occupied by a CO ligand in **RePBO-Me2(b)**. For the latter complex, the benzoxazole heterocycle can also be positioned in two different ways (in a 60/40 ratio) when considering the respective positions of the oxygen and nitrogen atoms. Regarding the intermolecular arrangement, for both types of crystals, all PBO units are displayed on parallel planes. The carbonyl groups and the halogen atom play an important role in structuring the network. For pure complex **RePBO-Me2(a)**, overlaps are observed between two PBO moieties distant by 3.7 Å, and between the pyridyl ring of one molecule and the triazole of the other one, although the centroid-to-centroid distance is quite large (3.9 Å) (Fig. S13). In solvate **RePBO-Me2(b)**, the solvent molecules form bulky clusters. A small superimposition of the triazole rings, which are quite close (3.5 Å), and a significant overlap of two PBO units, also distant by 3.5 Å, can be observed (Fig. S14). The overlap of aromatic systems is therefore more important in both types of crystals of complex **RePBO-Me2** than for **RePBO-Me1**.

Regarding **RePBO-Me3**, the asymmetric unit comprises a molecule of methanol and a molecule of complex crystallizing in the *P*bcn space group. Remarkably, the two methyl groups are situated at opposite faces of the organic ligand, probably to avoid mutual steric hindrance. The phenyl-triazole angle (α) is 63° while the pyta moiety is slightly twisted (β ~ 16°). Considering the whole set of molecules, the PBO units are displayed on two very different planes, where they take distinct orientations. Small overlaps are observed between a the pyridyl ring of one molecule and the PBO benzene ring of its neighbor, like if molecules form sort of antiparallel dimers, as well as between pyridyl and triazole, with a distance of the order of 3.4–3.5 Å (Fig. S15). A solvate of chloroform was also obtained by evaporation of a solution of **3** in this solvent, but the poor-quality structure is not reported here. However, it is clear that the geometry of the molecule is almost the same (phenyl-triazole angle α = 67° and angle β = 16°), even if the arrangement is quite different (space group: $P2_1/n$), all PBO units being located in parallel planes.

A common feature of all these structures is that two enantiomers, in identical proportions, coexist in the crystal cell. They differ by the position of the organic ligand with respect to the chlorine atom (see example in Fig. S16). However, it is noticeable that the chlorine atom faces the PBO unit above the plane formed by the pyta moiety, in almost every case. The only exception is the **RePBO-Me2(b)** solvate, where a CO ligand faces the PBO unit. Besides, it is clear that the presence of the methyl groups impacts significantly the geometry of the complexes. The main features are collected in Table 2. In **RePBO**, the PBO unit and triazole ring are close to perpendicular (α = 83.3°) and the pyta

fragment is almost planar (β ~ 8.6°) [15]. For the four complexes, the phenyl-triazole angle α was therefore decreased in the order: **RePBO** > **RePBO-Me1** > **RePBO-Me3** > **RePBO-Me2**. Remarkably, the pyridine-triazole angle β was increased as **RePBO-Me1** < **RePBO** < **RePBO-Me3** < **RePBO-Me2**, suggesting that the deformation of the pyta fragment compensates for the tension generated by the methyl group on the pyridine ring. Unexpectedly, the substitution on pyridine alone causes the most important changes in the geometry of the complex. The packing mode of the three methylated complexes also differs from that of **RePBO**, in which pairs of molecules are arranged in a herringbone manner, with no overlap of the aromatic moieties.

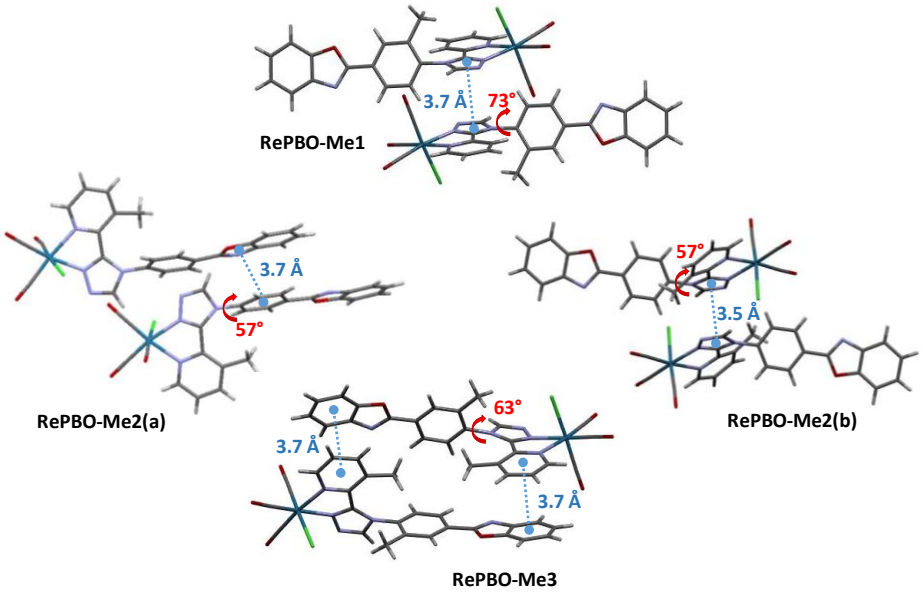

Fig. 1. Arrangement of two neighboring molecules in the crystal showing the phenyl-triazole dihedral angles α (red ink) and π-π interactions (blue dotted lines) for the methylated complexes. Blue balls represent the ring centroids *Cg*. Species **RePBO-Me2(a)** and **RePBO-Me2(b)** are the pure form and the dichloromethane solvate of **RePBO-Me2**, respectively.

Complex	Phenyl-triazole dihedral angle (α) [°]	Pyridyl-triazole dihedral angle (β) [°]	Intermolecular arrangement
RePBO-Me1	72.9	3.6	Slipped parallel
RePBO-Me2	56.3-57.0 [a] 56.9 [b]	19.5-20.1 [a] 24.3 [b]	Slipped parallel
RePBO-Me3	66.5	15.7	Slipped anti-parallel dimers
RePBO	83.3	8.6	Herringbone anti-parallel dimers

Table 2. Values of the phenyl-triazole (α) and pyridyl-triazole (β) dihedral angles, and type of intermolecular arrangement for the four complexes. *a*: Two molecules in the asymmetric unit of **RePBO-Me2(a)**. *b*: Dichloromethane solvate (**RePBO-Me2(b)**).

3.3. Electronic structures and transitions

Computational studies based on the density functional theory (DFT) and time-dependent DFT (TD-DFT) methods were performed for the three methylated complexes in dichloromethane. The full results are collected in the ESI (Tables S3–10, Fig. S17–23). Noticeably, the geometry calculated by DFT for the ground-state molecules in solution differs from that determined by XRD analysis for the molecules in the crystal: the benzoxazole moiety is positioned in such a way that the methyl group faces a carbonyl ligand, not to the chlorine atom (vide infra §3.4). As shown in Fig. 2, the composition of the two highest occupied molecular orbitals (HOMO and HOMO+1) is very similar in the three molecules:

the electron density is localized on the rhenium atom in the d^6 electronic configuration, the carbonyl ligands and the halogen atom. Small differences appear between the three complexes if considering the composition of the lowest unoccupied molecular orbitals LUMO and LUMO+1 (Table S9). For instance, for the compounds **RePBO-Me1** and **RePBO-Me3**, the electron density of the LUMO is mainly concentrated on the pyta moiety, and that of the LUMO+1 is on the PBO unit. For **RePBO-Me2**, the electron density is distributed more evenly over the whole organic ligand, the pyta and PBO fragments being respectively involved in approximately a 4:1 and 1:4 ratio in the LUMO and LUMO+1, respectively. This trend follows the evolution of the phenyl-triazole angle (α). The HOMO-LUMO gaps are very close, *i.e.* 4.01, 3.98 and 3.99 eV for **RePBO-Me1**, **RePBO-Me2** and **RePBO-Me3**, respectively.

For the three complexes, the lowest energy transition associated with high oscillation strength is a HOMO-1→LUMO transition with preponderant metal-to-ligand charge-transfer (MLCT) character and minor halide-to-ligand charge-transfer (XLCT) character. The high-energy transitions mainly have intra-ligand charge-transfer (ILCT) or MLCT character, as well as mixed character with XLCT contribution (Tables S4, S6 and S8). For some transitions, small differences appear between compounds. For example, the HOMO-2→LUMO, which has ILCT character, is more intense and at lower energy for **RePBO-Me2** and **RePBO-Me3** than for **RePBO-Me1.**

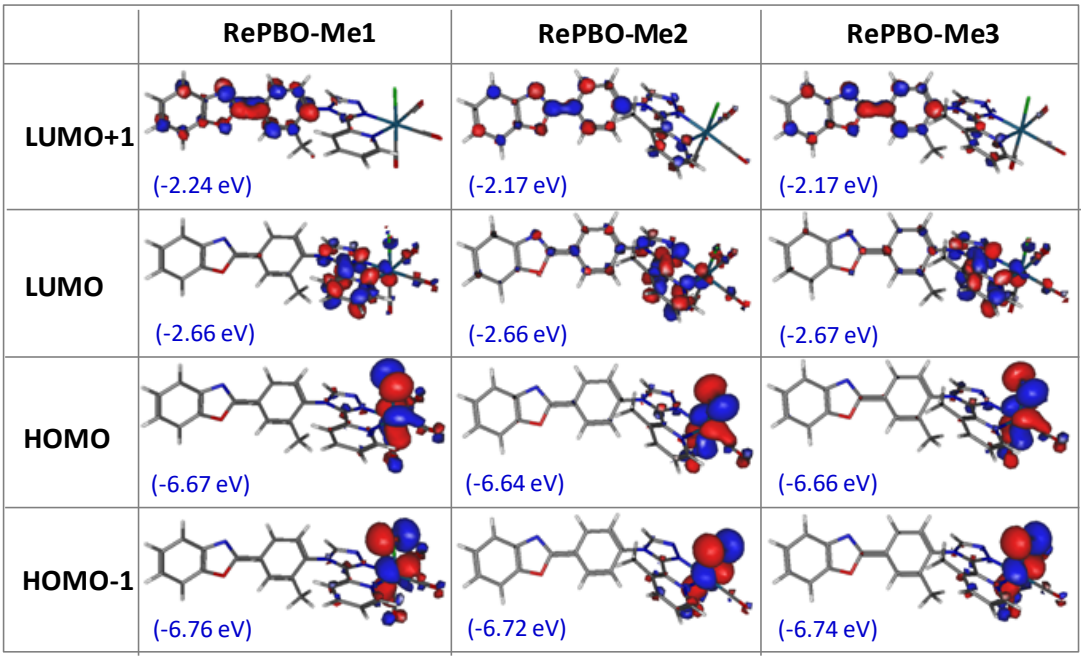

Fig. 2. Isodensity plots (isovalue = 0.03 e $bohr^{-3}$) and energy levels of the first frontier molecular orbitals, for the three methylated complexes in dichloromethane, according to DFT calculations at the PBE0/LANL2DZ level of theory.

Two low-lying triplet excited states with very close energy levels were also characterized, as is the case for **RePBO** [18]. The lowest-energy triplet state has MLCT character, the spin density distribution is localized on the pyta moiety and carbonyl ligands (Fig. S21). The second triplet state has ILCT character with the spin density distribution centered on the PBO unit (Fig. S22). There is no significant difference between the three complexes, except that the phenyl-triazole dihedral angle (α) gradually varies by ~15° as **RePBO-Me1** and **RePBO-Me2** pass from the ground state to the ^{3}ILCT excited state, and then to the ^{3}MLCT state, whereas the geometry of **RePBO-Me3** is virtually unchanged (Fig. S23 and Table S10).

3.4. ^{1}H NMR study

Data from ^{1}H NMR spectrometry give information about the rotation of the PBO unit with respect to the pyta moiety for the complexes in solution. Initially, the comparison of the spectra of the

three compounds in $CDCl_3$ at room temperature revealed interesting differences (Fig. 3, S2, S5 and S8). The spectrum of **RePBO-Me2** shows only one signal per proton. Besides, the H_{11} and H_{15} protons, on the one hand, and the H_{12} and H_{14} protons, on the other hand, appear as a broad unresolved signal centered at 8.50 ppm and 7.60 ppm, respectively. These protons are chemically but not magnetically equivalent, and the fact that they are indistinguishable suggests the fast rotation of the PBO unit at room temperature. In contrast, several signals, for example those corresponding to the pyridyl protons H_{24} and H_{25}, are more complicated for **RePBO-Me1** and **RePBO-Me3** than for **RePBO-Me2**. Some of them are clearly duplicated, like the singlet of the triazole proton H_{17}, the signals of H_{14}, H_{11} and H_{15}, the singlet of the methyl group borne by the phenyl ring (H_{27}) and, for **RePBO-Me3**, that of the methyl group borne by the pyridyl ring (H_{28}). Noticeably, the signals that exhibit the largest gap between them are observed for **RePBO-Me3**. For example, the doublets assigned to H_{14} and $H_{14'}$ on the one hand, and the singlets of H_{27} and $H_{27'}$ on the other hand, are separated by more than 0.23 ppm for **RePBO-Me3** *vs.* ~0.06 and 0.08 ppm, respectively, for **RePBO-Me1**. Similar trends are observed in the ^{13}C NMR spectra. These observations indicate the presence at room temperature of at least two stable conformers in a 65/35 and 50/50 ratio for **RePBO-Me1** and **RePBO-Me3**, respectively, as calculated from the integration of the signals.

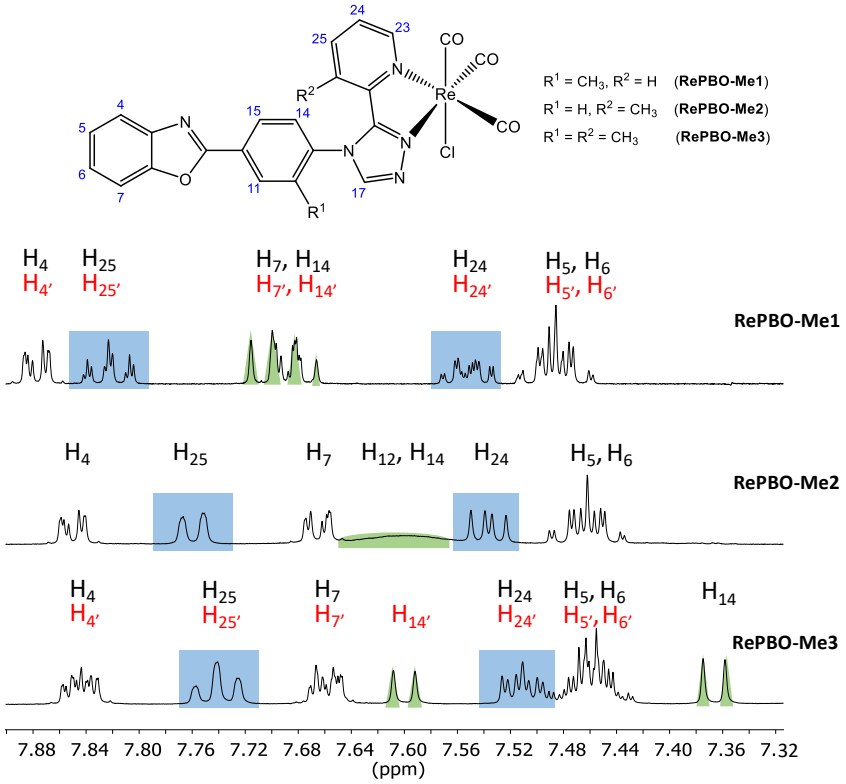

Fig. 3. Numbering of the main protons and comparison of the ^1H NMR spectra of **RePBO-Me1**, **RePBO-Me2** and **RePBO-Me3** in $CDCl_3$ at 25°C (500 MHz).

In a second time, variable temperature ^1H NMR spectrometry was implemented. For **RePBO-Me2** dissolved in CD_2Cl_2, the spectra were recorded by lowering the temperature between 283 and 203 K (Fig. 4). It was chosen to observe the signals of H_{11} and H_{15} because they do not overlap with other signals, unlike those of the H_{12} and H_{14} protons. At 258 K, two well-distinct doublets appear. The H_{11} and H_{15} protons thus have different chemical shifts with coupling constants $J(H_{11}\text{-}H_{12})$ and $J(H_{15}\text{-}H_{14})$ of 7 Hz. At 243 K, both doublets were split with a new coupling constant $J(H_{11}\text{-}H_{15})$ of 2Hz. It is therefore necessary to lower drastically the temperature so that the spectrum of **RePBO-Me2** becomes qualitatively similar to that of the other compounds at room temperature.

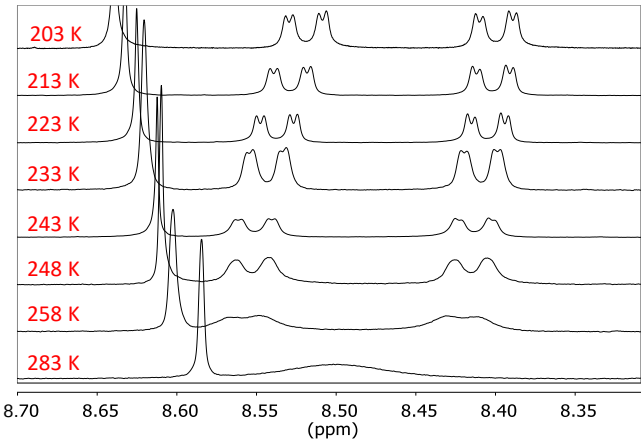

Fig. 4. Variable temperature ^{1}H NMR spectra of complex **RePBO-Me2** in CD_2Cl_2 (400 MHz), showing the separation of the signals corresponding to the H_{11} and H_{15} protons.

For the latter two complexes, the temperature was increased between 333K and 373K for **RePBO-Me1** in DMSO-d_6, and between 303 and 343K for **RePBO-Me3** in tetrachloroethane-d_2. In doing so, the signals corresponding to the methyl group borne by the phenyl ring got slightly closer, without any other significant change in the spectra (Fig. S11–12). These observations suggest that intramolecular blockages remain even when rising temperature.

The conformers detected in solutions of **RePBO-Me1** and **RePBO-Me3** were not identified. However, it can be hypothesized that one of them corresponds to the molecules described by the crystallographic studies, where the PBO unit faces the chlorine atom. The other conformer could then correspond to the molecules in which the PBO unit has undergone a rotation of 180° and faces a carbonyl ligand, *i.e.* the most stable species in solutions according to DFT calculations (Fig. 5). These two conformers could be close from an energetic point of view, as it is the case for **RePBO** [18]. Another argument in this direction is that the distance between the methyl group borne by the phenyl ring and the chlorine atom that faces it is quite short, *ca.* 3.6 Å for **RePBO-Me1** and only 3.3 Å for **RePBO-Me3**. For the second type of conformer, the distance between the methyl group and the carbonyl ligand is much longer (≥ 4.3 Å). It can be inferred that the H_{27} and H_{14} protons strongly feel the influence of the ligand facing them through space. This is well in line with the NMR results, which show that the environment of these protons is significantly impacted by the conformational change, especially for **RePBO-Me3**. In every case, the whole crystallographic and theoretical results indicate that many conformers/enantiomers are possible, due to the structure and various degrees of freedom of the molecules. Only a very thorough study, much beyond the scope of the present work, would allow differentiating them. The present ^{1}H NMR study only indicates that the three complexes differ by their flexibility. The methyl group interferes less with the rotation of the PBO fragment when inserted on the pyridine ring of **RePBO-Me2** than when situated on the phenyl ring of **RePBO-Me1** and **RePBO-Me3**.

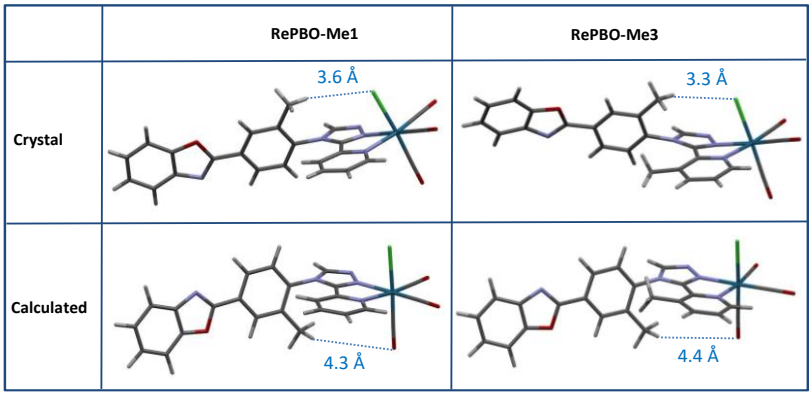

Fig. 5. Comparison between the molecular views of **RePBO-Me1** and **RePBO-Me3** drawn according to the results of crystallography and DFT calculations (only one enantiomer represented).

3.5. Electrochemical studies

The electrochemical behavior of the three methylated complexes was studied by cyclic voltammetry (CV) and Osteryoung square wave voltammetry (OSWV) measurements in DCM at room temperature (Tables S11–12, Fig. S24–32), and the results were compared with those previously published for other compounds of this family. The introduction of methyl group(s) into the initial framework of **RePBO** slightly influences the first oxidation potential of the compound centered on the Re atom [14, 15], as observed in OSWV (Fig. 6). The width of the other oxidation processes is smaller than that of the unsubstituted compound.

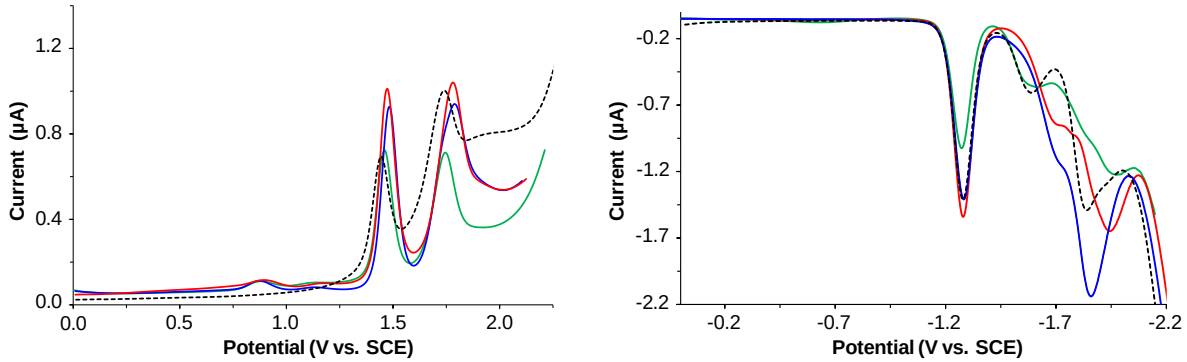

Fig. 6. OSWVs anodic (left) and cathodic (right) scans of complexes **RePBO-Me1** (blue), **RePBO-Me2** (green), **RePBO-Me3** (red), and **RePBO** (black) on a Pt electrode in CH_2Cl_2 + 0.1 M [nBu$_4$N][BF_4] at room temperature (frequency 20 Hz, amplitude 20 mV, step potential 5 mV).

In reduction, the first reduction process centered on the pyta moiety is also not significantly modified by the presence of one or two methyl groups in the new compounds. Compounds **RePBO-Me1** and **RePBO-Me3** incorporating a methyl group on the phenyl moiety exhibit several similar broad reduction processes ranging from −1.68 V to −1.94 V (Table S11). Compound **RePBO-Me2** bearing a methyl group on the pyridine ring shows some differences when compared to the other complexes. Indeed, a second reduction process of medium intensity (at −1.56 V) is observed like for **RePBO**, and its other reduction processes appear as less broad waves. It is noteworthy that a minor contribution of dichloromethane cannot be ruled out as its first reduction process of very weak intensity could be observed at −1.60 V under the same conditions. However, for **RePBO-Me1** and **RePBO-Me3**, all the reduction processes above −1.3 V can be mainly attributed to those involving the benzoxazole moiety [14, 15]. In particular, they are not observed in the benzoxazole-free counterparts [16, 17]. Moreover, CVs examination at different scan rates also indicate that the three compounds possess very close electrochemical characteristics when compared to **RePBO**. For example, a 1/1 intensity ratio for the first one-electron oxidation and the first one-electron reduction processes is evidenced, and the latter is also quasi-reversible around 0.5 V/s in each case (Fig. S24–25, S27–28, S30–31).

Finally, the estimated values of the electrochemical gap (Eg^{el}) of these three compounds (≈ 2.52 eV) are also very close to that of **RePBO** (2.50 eV), and in good agreement with those of the calculated HOMO-LUMO gap (E_{calc}) (≈ 2.94 eV) (Table S12). Given the similarities between the electrochemical behavior of the new complexes and that of **RePBO**, it can be concluded that the presence of methyl group(s) does not significantly affect the electronic processes occurring in solution.

3.6. UV-visible absorption and emission spectral properties

Solutions of the methylated complexes in dichloromethane were yellow in daylight. The experimental absorption spectra were very close (Fig. 7 and Table 3) and in good agreement with the simulated ones (Fig. S20). The low-energy band of MLCT character was almost superimposable for the three compounds, while the high-energy absorption band, mainly attributed to intra ligand (IL)

transitions, was slightly shifted to the red in the order **RePBO-Me1** < **RePBO-Me3** < **RePBO-Me2**. The molar extinction coefficients were slightly increased in the same order. The solutions were weakly emissive in the orange-red under UV light (365 nm). Again, the maximum of the single unresolved band was shifted to the red when passing from **RePBO-Me1** (626 nm) to **RePBO-Me3** (634 nm), and then to **RePBO-Me2** (640 nm). The experimental values were in rather good agreement with those calculated by DFT considering the involvement of the lowest ^{3}MLCT state (608, 635 and 630 nm, respectively), which confirms that emission is due to phosphorescence. These spectroscopic features can be related to the planarity of the molecules, and thus to the increase of electron conjugation in the order **RePBO-Me1** < **RePBO-Me3** < **RePBO-Me2**. The rather low quantum yields were decreased in the reverse order, as were the monoexponential lifetimes, which passed from 70 to 54 ns. **RePBO-Me2** is therefore the least emissive species. The fact that it has the highest non-radiative rate constant is in line with the NMR results, which indicates that intramolecular rotations are easier in this complex than in the other two. However, the photophysical constant values are so close for the three complexes that they must be discussed with caution. It is noteworthy that the presence of isomers in **RePBO-Me1** and **RePBO-Me3** was not detected by optical spectroscopy. Overall, the three methylated complexes in solution exhibit a very similar behavior, which is also very close to that of **RePBO**.

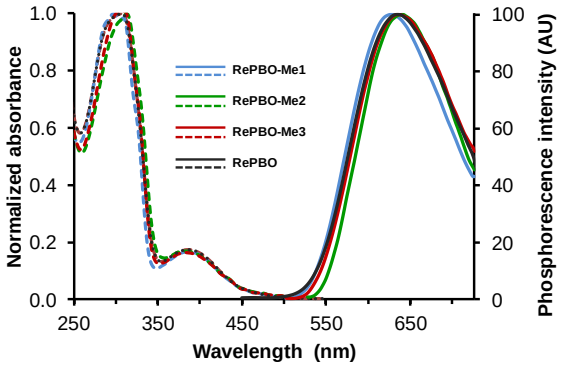

Fig. 7. UV-vis absorption spectra (slashed lines) and normalized emission spectra (solid lines) of complexes **RePBO-Me1** (blue line), **RePBO-Me2** (green line) and **RePBO-Me3** (red line) and **RePBO** (black line) in undegassed dichloromethane. Concentrations ~ 3.3×10^{-5} M for absorption, 1.2×10^{-5} M for emission. Excitation at the maximum wavelength of the low-energy absorption band.

Complex	λ_{abs} [nm]	ε [$M^{-1}cm^{-1}$]	λ_P [nm]	Φ_P	τ [ns]	χ^2	k_r [s^{-1}]	k_{nr} [s^{-1}]
RePBO-Me1	298 388	28600 4600	626	0.018	70	1.38	2.6×10^5	1.4×10^7
RePBO-Me2	310 382	31800 5300	640	0.013	54	1.40	2.4×10^5	1.8×10^7
RePBO-Me3	308 382	30400 4800	634	0.017	62	2.27	2.7×10^5	1.6×10^7
RePBO [a]	310 388	29600 5100	632	0.012	80	1.19	1.5×10^5	1.5×10^7

[a] From ref. [15].

Table 3. Spectroscopic data of the three methylated complexes and **RePBO** in dichloromethane solution. Maximum absorption wavelength (λ_{abs}) and molar extinction coefficient (ε), maximum emission wavelength (λ_P), quantum yield (Φ_P) and lifetime (τ) with chi square (χ^2) values; radiative (k_r) and non-radiative (k_{nr}) deactivation constants. Solution concentrations: ~ 3.3×10^{-5} M for absorption, ~ 1.2×10^{-5} M for emission. Excitation near the maximum wavelength of the low-energy ^{1}MLCT band. Decays are given in Fig. S33−35.

The effect of aggregation on the photoluminescence properties was investigated by increasing the water proportion in an acetonitrile solution of the complexes (Fig. 8). The three complexes emitted weak orange-red light in pure acetonitrile. Their photoluminescence intensity was increased weakly when the water proportion in acetonitrile passed from 0 to 60%, then strongly up to 80 or 90%, and

finally it was decreased abruptly for high water proportions. This intensity change was accompanied by a significant color change of the emitted light, and by the appearance of small particles visible to the naked eye. Remarkably, the aggregation-induced emission (AIE) effect was quite different according to the compound. It was particularly strong for **RePBO-Me1**, whose aggregated samples emit intensely in the yellow-green. Indeed, the spectra shifted up to 544 nm, which corresponds to a blue-shift of 80 nm with respect to pure acetonitrile. At this wavelength, the intensity of the PL signal was multiplied up to 56 times. At the maximum of the most intense band (558 nm), it was multiplied by 40. **RePBO-Me2**

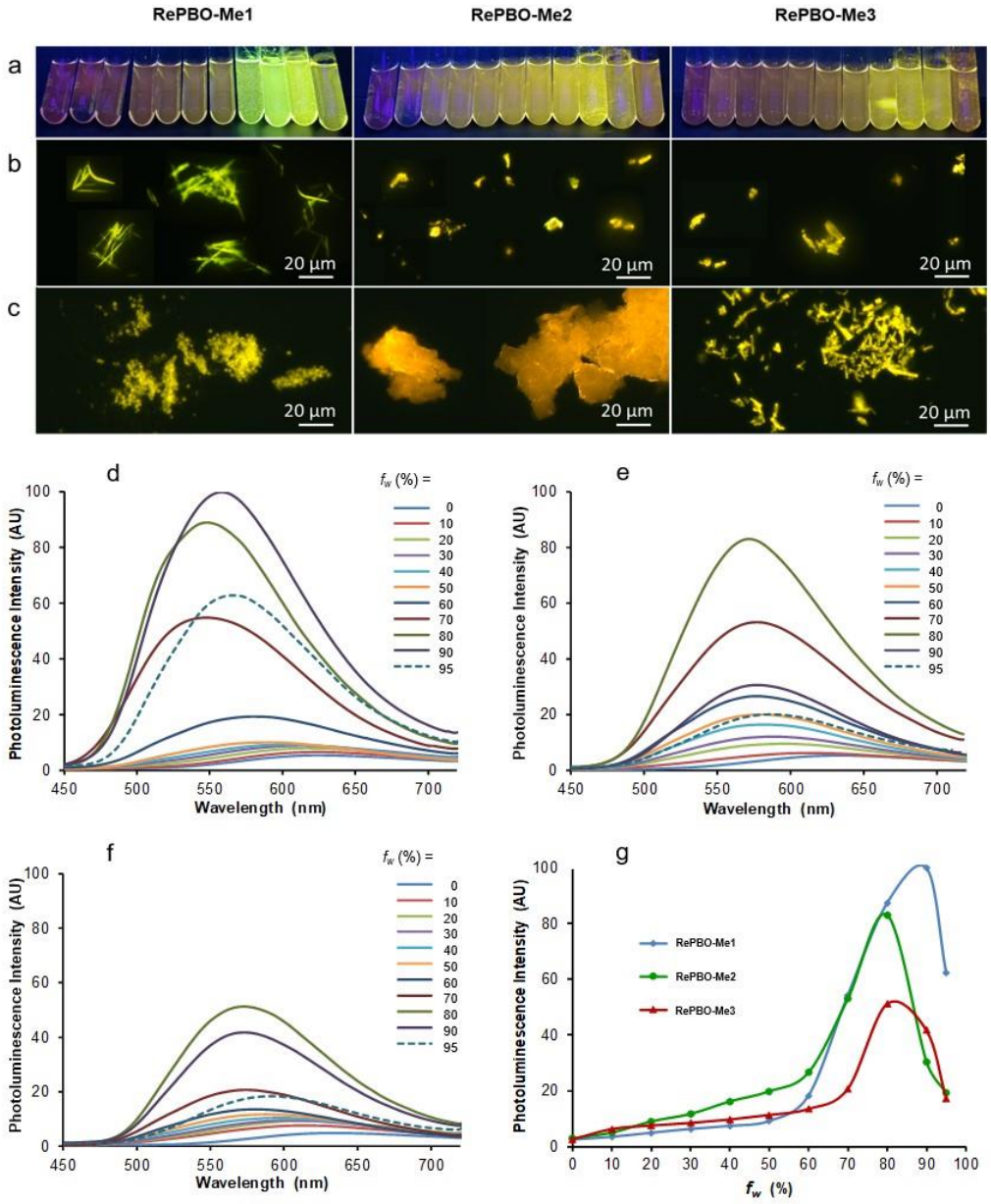

Fig. 8. a) Samples of the three methylated complexes at ~3.6×10^{-5} M in acetonitrile solutions containing from 0 to 95% water (from left to right), under illumination at 365 nm. b,c) Fluorescence microscopy images of the samples containing 80% (b) and 95 % water (c). d-e) Corresponding emission spectra (λ_{ex} = 350 nm) for **RePBO-Me1** (d), **RePBO-Me2** (e) and **RePBO-Me3** (f). g) Compared evolution of the PL intensity at 558 nm (**RePBO-Me1**) and 572 nm (**RePBO-Me2** and **RePBO-Me3**) as a function of the water fraction (f_w). Normalization with respect to the emission intensity in acetonitrile solutions.

and **RePBO-Me3** led to less spectacular variations. The light emitted by the suspensions was yellow (572 nm) and the maximum blue-shift with respect to acetonitrile was only 62 nm. The intensity was increased 27 times for **RePBO-Me2** and 20 times for **RePBO-Me3** with respect to acetonitrile solutions. For the three compounds, the observation by fluorescence microscopy of the samples containing 80% water revealed the presence of intensively luminescent microcrystals: needle-like crystals that emit in the yellow-green for **RePBO-Me1**, platelets emitting in the yellow for the other two complexes (Fig. 8b). The shape and color of the detected objects was quite different in the samples containing 95% water, in particular for **RePBO-Me1** and **RePBO-Me2** that lead to agglomerates of very thin particles, the crystallinity of which cannot be ascertained (Fig. 8c). Possibly, these particles form very quickly in the presence of high amounts of water, and could explain the reverse wavelength shift and the weaker PL signal observed for these samples with respect to those containing a little less water. An evolution of the respective intensities of the spectra was observed after 48 h, probably related to slow growth of the microcrystals. By comparison, **RePBO** shows a clear AIE effect with a maximum blue shift of 78 nm and multiplication of the emission signal by 23 at the maximum of the most shifted band (Fig. S36) [15]. Not only **RePBO-Me1** resembles its parent compound, but it exhibits a better AIE affect, while the other two complexes are noticeably less effective.

Solid samples were then considered (Table 4). The observation with the fluorescence microscope showed that the as-synthesized powders of the three complexes are microcrystalline (Fig. S37). Under UV illumination (365 nm), they emitted yellow to golden-yellow light. The excitation spectra showed that the ^{1}MLCT band has moved to the visible range, between 400 nm and 500 nm (Fig. S38−40). The emission spectra peaked between 549 and 570 nm (Fig. 9). The photoluminescence quantum yields (PLQY) were between 0.18 and 0.36. Two main lifetimes were detected, the value of which varies widely with the compound, and the longest of which is systematically associated with the preponderant fraction of intensity. In our former work, these two lifetimes were attributed to the concomitant contribution of the ^{3}ILCT and ^{3}MLCT excited states [18]. By comparison, **RePBO** emits bright green-yellow light at shorter wavelength (542 nm) and with a stronger PLQY (0.55), and its lifetime is intermediate between those of the methylated complexes. In summary, all four complexes show clear crystallization-induced emission enhancement (CIEE), with significant differences between them.

The similarity between the spectra of the microcrystalline powders and those of the aggregate suspensions formed with 80% water, whose main emissive species are microcrystals, is obvious. In both cases, the main factor responsible for emission enhancement is the restriction of intramolecular motions, which prevents the molecules from deactivating on a non-radiative mode [9–13], generally through conical intersections [36, 37]. To a lesser extent, the prevention of quenching by oxygen also plays a role. Favorable crystal packing modes must be added. Since the four complexes exhibit close spectroscopic properties in solution, the differences observed in the solid state arise from specific factors, such as the molecular conformation and the intermolecular interactions that take place in crystals [3], Indeed, the X-ray analysis has shown that they vary considerably according to the substitution pattern. These data allow the behavior of the microcrystalline powders to be discussed, but the crystallinity may be different in the aqueous suspensions. For the powders, it can be noticed that the emission spectra shift to long wavelengths when the planarity of the organic ligand increases. The evolution of the PLQY is more delicate to understand. It is neither related to the ligand planarity nor to the overlap of the aromatic moieties of adjacent molecules. In particular, **RePBO** and **RePBO-Me1**, which exhibit respectively the highest and the lowest PLQY, have close geometries and show no overlap of their aromatic moieties in the crystals. However, the molecules are displayed as herringbone for the first compound and as layers for the second one, and it can be thought that intermolecular interactions, and hence the stabilization of the emitting states, are different in both cases. On the other hand, the emission efficiency of the **RePBO-Me1** microcrystalline powder is lower than might have been expected from the AIE experiments, which confirms that crystallinity and the number of defects [3] must play an important role.

Complex	AIE [b]	Pristine microcrystalline powder							Ground powder							THF-Fumed powder		
	λ_{PL} [nm]	λ_{PL} [c] [nm]	Φ_{PL} [d]	τ [c] [ns] (f) [%]	$<\tau>$ [ns]	χ^2	k_r [s^{-1}]	k_{nr} [s^{-1}]	λ_{PL} [c] [nm]	$\Delta\lambda_{PL}$ [nm]	Φ_{PL} [d]	τ [c] [ns] (f) [%]	$<\tau>$ [ns]	χ^2	k_r [s^{-1}]	k_{nr} [s^{-1}]	λ_P [c] [nm]	Φ_P [d]
RePBO-Me1	544	549	0.18	89 (0.18) 347 (0.79)	289	1.06	6.2×10^5	2.8×10^6	597	48	0.06	56 (0.25) 243 (0.67)	177	1.07	3.4×10^5	5.3×10^6	554	0.19
RePBO-Me2	572	570	0.29	126 (0.15) 525 (0.81)	447	0.90	6.5×10^5	1.6×10^6	605	35	0.09	65 (0.26) 260 (0.69)	197	1.04	5.6×10^5	4.5×10^6	564	0.25
RePBO-Me3	572	563	0.36	155 (0.14) 748 (0.84)	648	0.86	5.6×10^5	9.9×10^5	600	37	0.14	53 (0.36) 248 (0.56)	159	1.00	8.9×10^5	5.4×10^6	564	0.30
RePBO [a]	558	542	0.55	93 (0.12) 563 (0.85)	490	---	1.1×10^6	9.2×10^5	600	58	0.25	60 (0.14) 260 (0.82)	220	---	1.1×10^6	3.4×10^6	542	0.55

[a] From ref. [15] and [18]; [b] Water/acetonitrile 80:20; [c] λ_{ex} = 420 nm; [d] λ_{ex} = 380 nm.

Table 4. Spectroscopic data of the three methylated complexes and **RePBO** in the various solid states, *i.e.* microcrystals and aggregates formed in aqueous suspension (AIE experiment), microcrystalline pristine powder, ground powder, ground powder subsequently fumed with THF vapors. Maximum emission wavelength (λ_{PL}); quantum yield (Φ_{PL}) and lifetime (τ) with fractions of intensity (f), weighted average lifetimes $<\tau>$, and chi square (χ^2) values; radiative (k_r) and non-radiative (k_{nr}) deactivation constants. Decays are given in Fig. S41−46.

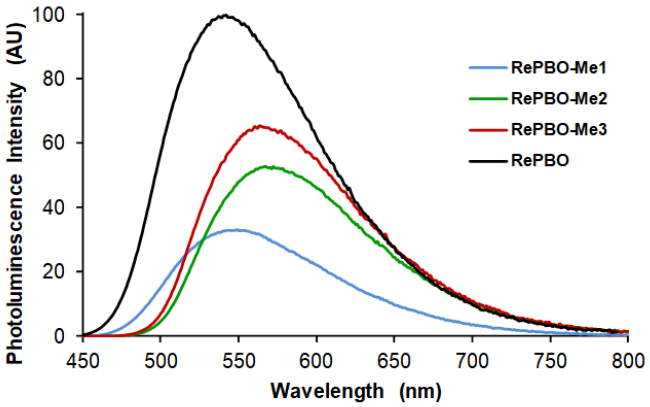

Fig. 9. Photoluminescence spectra of the four complexes as microcrystalline pristine powders, with the intensity at the emission maximum proportional to PLQY. **RePBO-Me1** (blue line), **RePBO-Me2** (green line) and **RePBO-Me3** (red line), **RePBO** (black line). λ_{ex} = 420 nm.

Finally, the mechanoresponsive luminescence properties were investigated (Fig. 10). Grinding with a mortar and a pestle led to red-shifts of 35, 37 and 48 nm for complexes **RePBO-Me2**, **RePBO-Me3** and **RePBO-Me1**, respectively, accompanied by a decrease of the PLQY and average lifetimes. These effects were almost reversible upon fuming with THF vapors. Qualitatively, the methylated complexes behave like **RePBO**, for which the observed effects have been related to the amorphization of the samples upon grinding, and to the recovery of crystallinity upon solvent fuming on the bases of powder X-ray diffraction analyses [18]. In the present case, it can be checked by fluorescence microscopy that the disappearance of microcrystals upon grinding is accompanied by a red-orange emission (Fig. S37). All these complexes are thus particularly sensitive to any change in the intermolecular interactions and packing constraints. However, two striking features emerge. The first one is that the amplitude of the MRL effect, *i.e.* the wavelength shift observed after grinding, is significantly smaller for the methylated complexes than for **RePBO** ($\Delta\lambda_{PL}$ = 58 nm). The second one is that the maximum emission wavelength and lifetimes of the three methylated complexes and **RePBO** are almost similar in the amorphous phase, where packing constraints are weaker and molecular motions more easily allowed than in crystals. Consequently, the amplitude of the MRL effect depends on the spectroscopic characteristics of the native powders, and therefore on the particular geometry of the

molecules in the crystals: the closer the phenyl-triazole dihedral angle (α) is from 90° for the pristine powder, the stronger the MRL effect. Figure 10c shows that these two parameters correlate quite well.

To the best of our knowledge, no correlation between a geometrical parameter and the amplitude of the MRL effect has been reported for rhenium complexes and closely related transition metal complexes, for which this type of studies is still quite rare. As is the case for organic compounds [38, 39], MRL-active materials based on transition metal complexes mainly rely on the change of molecular packing patterns and intermolecular interactions, although original mechanisms like metallophilic interactions and the switching between excited states can also take place [6–8]. The variation of a precise geometrical parameter is rarely evoked. However, studies on polymorphic compounds have shown for a long time that conformational changes have a significant effect on the PL and mechanochromic properties of organic compounds [40–44]. Our original result will have to be confirmed with a greater number of complexes and interpreted using relevant theoretical calculations.

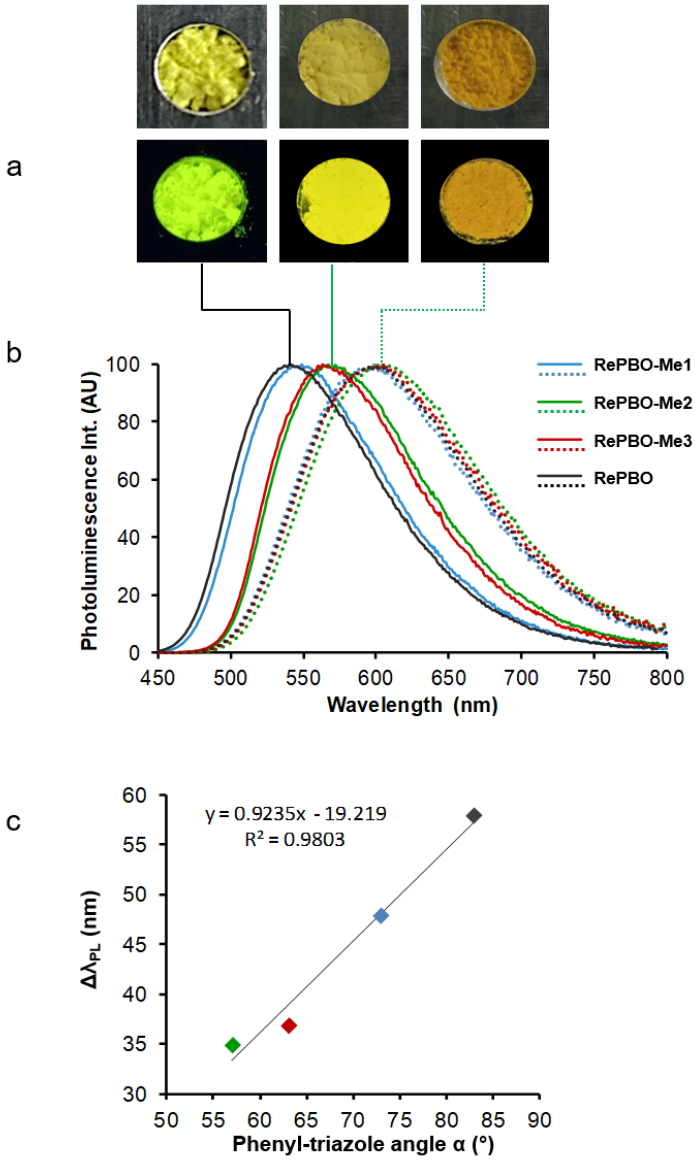

Fig. 10. a) From left to right: images of the microcrystalline pristine powders of **RePBO** and **RePBO-Me2**, and ground powder of **RePBO-Me2**, in the daylight (top) and under illumination at 365 nm (bottom). b) Normalized PL spectra of the four complexes as microcrystalline pristine powders (solid lines) and ground powders (dotted lines). c) Correlation between the wavelength shift induced by grinding and the phenyl-triazole dihedral angle (α) of the molecules. For PL spectra: **RePBO-Me1** (blue line), **RePBO-Me2** (green line) and **RePBO-Me3** (red line), **RePBO** (black line). λ_{ex} = 420 nm.

CONCLUSIONS

A trifling effect could have been expected from small chemical modifications like the insertion of one or two methyl groups on the organic ligand of **RePBO**. The electronic effect is indeed relatively weak, but a steric hindrance effect was detected. According to NMR experiments, the rotation of the PBO unit is more hindered when a methyl group is placed on the phenyl ring than when it is on the pyta moiety. However, there was little impact on the properties in solutions, where the unsubstituted **RePBO** complex and its three methylated analogues behaved almost similarly. This was no longer the case in the various solid states, where all compounds showed clear solid-state enhancement effect. The presence of the methyl group(s) strongly affects the molecular geometry and packing mode in the crystals. Consequently, the PL properties of the aggregate suspensions (containing mainly microcrystals) formed in the presence of water, and those of the pristine microcrystalline powders drastically depended on the substitution pattern. The emission of the powders was sensitive to mechanical stimuli. Remarkably, in the amorphous state where molecules regain their mobility, differences between them were much reduced. It appeared therefore that the amplitude of the MRL effect correlates well with the geometry of the molecules in the pristine powder. It is inferred from this work that the unsubstituted compound **RePBO** is the most efficient if MRL properties are sought after, while a small substitution on the phenyl ring (**RePBO-Me1**) enhances the AIE-effect.

This study provides a better understanding of the behavior of photoluminescent tricarbonylrhenium(I) complexes, taken as molecular prototypes. In a much broader way, it shows how minor structural differences can modulate solid-state emission properties, and how difficult it is to predict them. As a result, this study is one more step towards the rational design of increasingly efficient PL materials, which are actively sought after, but also very little known, especially when it comes to transition metal complexes.

Acknowledgements

ANR is gratefully acknowledged for funding (PANTHERA project # ANR-22-CE29-0008-1). We thank Dr. C.-L. Serpentini for his help in the measurement of PL lifetimes in solution, and Dr. Frédéric Rodriguez for his expertise in running softwares. We thank Dr. A. Sournia-Saquet and Mr. A. Moreau (LCC) for their help in electrochemical measurements. We are also indebted to Dr. Stéphane Massou and Ms. Caroline Toppan for the measurement of variable temperature NMR spectra.

Appendix A. Supplementary data

Experimental details including proton numbering for NMR, ^{1}H and ^{13}C NMR spectra, molecular views and crystallographic data, theoretical calculation data, electrochemical and spectroscopic data.

Appendix B.

CIF data

References

[1] J. Mei, N. L. C. Leung, R. T. K. Kwok, J. W. Y. Lam, B. Z. Tang, Aggregation-Induced Emission: Together We Shine, United We Soar! Chem. Rev. 115 (2015) 11718–11940.

[2] G. R. Suman, M. Pandey, A. S. J. Chakravarthy, Review on new horizons of aggregation induced emission: from design to development. Mater. Chem. Front. 5 (2021) 1541–1584.

[3] J. Gierschner, J. Shi, B. Milián-Medina, D. Roca-Sanjuán, S. Varghese, S. Y. Park, Luminescence in crystalline organic materials: From molecules to molecular solids. Adv. Opt. Mater. (2021) 2002251.

[4] S. Ito, Recent advances in mechanochromic luminescence of organic crystalline compounds. Chem. Lett. 50 (2021) 649–660.

[5] Z. Chen, H. Qin, Y. Yin, D. Deng, S.-Y. Qin, N. Li, K. Wang, Y. Sun, Full-Color Emissive D-D-A Carbazole Luminophores: Red-toNIR Mechano-fluorochromism, Aggregation-Induced NearInfrared Emission, and Application in Photodynamic Therapy. Chem. Eur. J. 29 (2023) e202203797.

[6] P. Xue, J. Ding, P. Wang, R. Lu, Recent progress in the mechanochromism of phosphorescent organic molecules and metal complexes. J. Mater. Chem. C 4 (2016) 6688–6706.

[7] X.-Y. Wang, L. Lv, L. Sun, Y. Hou, Z. Hou, Z. Chen, Recent advances in mechanochromism of metal-organic compounds. Front. Chem. 10 (2022) 865198.

[8] Y. Yin, Z. Chen, R.-H. Li, C. Yuan, T.-Y. Shao, K. Wang, H. Tan, Y. Sun, Ligand-Triggered Platinum(II) Metallacycle with Mechanochromic and Vapochromic Responses. Inorg. Chem. 60 (2021) 9387–9393.

[9] P. Alam, C. Climent, P. Alemany, I. R. Laskar, "Aggregation-induced emission" of transition metal compounds: Design, mechanistic insights, and applications. J. Photochem. Photobiol. C 41 (2019) 100317.

[10] P. Prasad, A. Gupta, P. K. Sasmal, Aggregation-induced emission active metal complexes: a promising strategy to tackle bacterial infections. Chem. Commun. 57 (2021) 174–186.

[11] X. Shi, X. Yan, H.-B. Yang, Aggregation-induced Emission (AIE) Active Metal–Organic Coordination Complexes, *in* Handbook of Aggregation Induced Emission. Y. Tang, B. Z. Tang Edts., Wiley on-line library, 2022, Ch. 14.

[12] L. Ravotto, P. Ceroni, Aggregation induced phosphorescence of metal complexes: From

principles to applications. Coord. Chem. Rev. 346 (2017) 62–76.

[13] S. Liu, Y. Pei, D. Zhu, AIE-based transition metal complexes for biological applications *in* Aggregation-Induced Emission, De Gruyter Edt., 2022, Ch. 20, Vol. 2.

[14] J. Wang, B. Delavaux-Nicot, M. Wolff, S. Mallet-Ladeira, R. Métivier, E. Benoist, S. Fery-Forgues, The unsuspected influence of the pyridyl-triazole ligand isomerism upon the electronic properties of tricarbonyl rhenium complexes: an experimental and theoretical insight. Dalton Trans. 47 (2018) 8087–8099.

[15] J. Wang, A. Poirot, B. Delavaux-Nicot, M. Wolff, S. Mallet-Ladeira, J. P. Calupitan, C. Allain, E. Benoist, S. Fery-Forgues, Optimization of aggregation-induced phosphorescence enhancement in mononuclear tricarbonyl rhenium(I) complexes: the influence of steric hindrance and isomerism. Dalton Trans. 48 (2019)15906–15916.

[16] A. Poirot, C. Vanucci-Bacqué, B. Delavaux-Nicot, N. Leygue, N. Saffon-Merceron, F. Alary, F. Bedos-Belval, E. Benoist, S. Fery-Forgues, Phenyl-pyta-tricarbonylrhenium(I) complexes: combining a simplified structure and steric hindrance to modulate the photoluminescence properties. Dalton Trans. 50 (2021) 13686–13698.

[17] A. Poirot, C. Vanucci-Bacqué, B. Delavaux-Nicot, N. Saffon-Merceron, C.-L. Serpentini, N. Leygue, F. Bedos-Belval, E. Benoist, S. Fery-Forgues, Luminescent fac-[ReX(CO)$_3$(phenyl-pyta)] (X = Cl, Br, I) complexes: influence of the halide ligand on the electronic properties in solution and in the solid state. Photochem. Photobiol. Sci. 22 (2023) 169−184.

[18] J. P. Calupitan, A. Poirot, J. Wang, B. Delavaux-Nicot, M. Wolff, M. Jaworska, R. Métivier, E. Benoist, C. Allain, S. Fery-Forgues, Mechanical modulation of the solid-state luminescence of tricarbonyl rhenium(I) complexes through the interplay between two triplet excited states. Chem. Eur. J. 27 (2021) 4191−4196.

[19] A. G. Yaremenko, D. M. Volochnyuk, V. V. Shelyakin, O. O. Grygorenko, Tetrahydropyrido[*d*]pyridazinones-promising scaffolds for drug discovery. Tetrahedron 69, (2013) 6799–6803.

[20] H. R. Hoveyda, G. L. Fraser, M. O. Roy, G. Dutheuil, F. Batt, M. El Bousmaqui, J. Korac, F. Lenoir, A. Lapin, S. Noel, S. Blanc, Discovery and optimization of novel antagonists to the human neurokinin-3 receptor for the treatment of sex-hormone disorders (part I). J. Med. Chem 58 (2015) 3060–3082.

[21] SADABS, Program for data correction, Bruker-AXS.

[22] G. M. Sheldrick, SHELXT-Integrated space-group and crystal-structure determination. Acta Cryst. A 71 (2015) 3–8.

[23] G. M. Sheldrick, Crystal structure refinement with SHELXL. Acta Cryst. C 71 (2015) 3–8.

[24] K. Suzuki, A. Kobayashi, S. Kaneko, K. Takehira, T. Yoshihara, H. Ishida, Y. Shiina, S. Oishi, S. Tobita, Reevaluation of absolute luminescence quantum yields of standard solutions using a spectrometer with an integrating sphere and a back-thinned CCD detector. Phys. Chem. Chem. Phys. 11 (2009) 9850–9860.

[25] J. C. De Mello, H. F. Wittmann, R. H. Friend, An improved experimental determination of external photoluminescence quantum efficiency. Adv. Mater. 9 (1997) 230–232.

[26] A.-R. Allouche, Gabedit-A graphical user interface for computational chemistry softwares. J. Comput. Chem. 32 (2011) 174–182.

[27] C. Adamo, V. Barone, Toward reliable density functional methods without adjustable parameters: The PBE0 model. J. Chem. Phys. 110 (1999) 6158–6170.

[28] J. P. Perdew, K. Burke, M. Ernzerhof, Generalized gradient approximation made simple. Phys. Rev. Lett. 77 (1996) 3865–3868.

[29] P. J. Hay, W. R. Wadt, Potentials for the transition metal atoms Sc to Hg. J. Chem. Phys. 82 (1985) 270–283.

[30] P. J. Hay, W. R. Wadt, *Ab initio* effective core potentials for molecular calculations. Potentials for K to Au including the outermost core orbitals. Chem. Phys. 82 (1985) 299–310.

[31] B. Mennucci, J. Tomasi, Continuum solvation models: A new approach to the problem of solute's charge distribution and cavity boundaries. J. Chem. Phys. 106 (1997) 5151–2158

[32] M. Cossi, V. Barone, B. Mennucci, J. Tomasi, *Ab initio* study of ionic solutions by a polarizable continuum dielectric model. Chem. Phys. Lett. 286 (1998) 253–260.

[33] M. Qin, X. Zhai, H. Xie, J. Ma, K. Lu, Y. Wang, L. Wang, Y. Gu, P. Gong, Design and synthesis of novel 2-(4-(2-(dimethylamino)ethyl)-4H-1,2,4-triazol-3-yl)pyridines as potential antitumor agents. Eur. J. Med Chem. 81 (2014) 47–58.

[34] C. Ainsworth, The condensation of aryl carboxylic acid hydrazides with orthoesters. J. Am. Chem. Soc. 77 (1954) 1148–1150.

[35] A. V. Kuttatheyil, M. Handke, J. Bergmann, D. Lassig, J. Lincke, J. Haase, M. Bertmer, H. Krautscheid, ^{113}Cd Solid-state NMR for probing the coordination sphere in metal-organic frameworks. Chem. Eur. J. 21 (2015) 1118–1124.

[36] R. Crespo-Otero, Q. Li, L. Blancafort, Exploring Potential Energy Surfaces for Aggregation Induced Emission-From Solution to Crystal. Chem. Asian J. 14 (2019) 700–714.

[37] Y. Chen, J. W. Y. Lam, R. T. K. Kwok, B. Liu, B. Z. Tang, Aggregation-induced emission: fundamental understanding and future developments. Mater. Horiz. 6 (2019) 428–433.

[38] P. S. Hariharan, V. K. Prasad, S. Nandi, A. Anoop, D. Moon, S. P. Anthony, Molecular engineering of triphenylamine based aggregation enhanced emissive fluorophore: Structure-dependent mechanochromism and self-reversible fluorescence switching. Cryst. Growth Des. 17 (2017) 146–155.

[39] M. Louis, A. Brosseau, R. Guillot, F. Ito, C. Allain, R. Métivier, Polymorphism, Mechanofluorochromism, and Photophysical Characterization of a Carbonyl Substituted Difluoroboron-β-Diketone Derivative. J. Phys. Chem. C 121 (2017) 15897–15907.

[40] K. Wang, H. Zhang, S. Chen, G. Yang, J. Zhang, W. Tian, Z. Su, Y. Wang, Organic polymorphs: One-compound-based crystals with molecular-conformation- and packing-dependent luminescent properties. Adv. Mater. 26 (2014) 6168–6173.

[41] H. Liu, Z. Lu, B. Tang, Z. Zhang, Y. Wang, H. Zhang, AIE-active organic polymorphs displaying molecular conformation-dependent amplified spontaneous emissions (ASE). Dye Pigm. 149 (2018) 284–289.

[42] X. Zhang, Q. Xu, Z. Chen, F. Li, F. Liu, J. Xu, G. Zhang, Effect of molecular conformation-changing on mechanochromism in tetraphenylethene substituted carbazole units. Mater. Chem. Phys. 289 (2022) 126462.

[43] C. Zhu, Q. Luo, Y. Shen, C. Lv, S. Zhao, X. Lv, F. Cao, K. Wang, Q. Song, C. Zhang, Y. Zhang, Red to near-infrared mechanochromism from metal-free polycrystals: Noncovalent conformational locks facilitating wide-range redshift. Angew. Chem. 60 (2021) 8510–8514.

[44] G. Zhang, J. Sun, P. Xue, Z. Zhang, P. Gong, J. Peng, R. Lu, Phenothiazine modified triphenylacrylonitrile derivates: AIE and mechanochromism tuned by molecular conformation. J. Mater. Chem. C 3 (2015) 2925–2932.